Annu. Rev. Earth Planet. Sci. 1998. 26:643–96

LABORATORY-DERIVED FRICTION LAWS AND THEIR APPLICATION TO SEISMIC FAULTING

Chris Marone
Department of Earth, Atmospheric, and Planetary Sciences, Massachusetts Institute of Technology, Cambridge, Massachusetts 02139; e-mail: cjm@westerly.mit.edu

KEY WORDS: earthquake faults, frictional properties and constitutive laws, physics of friction, granular fault gouge, earthquake afterslip

ABSTRACT

This paper reviews rock friction and the frictional properties of earthquake faults. The basis for rate- and state-dependent friction laws is reviewed. The friction state variable is discussed, including its interpretation as a measure of average asperity contact time and porosity within granular fault gouge. Data are summarized showing that friction evolves even during truly stationary contact, and the connection between modern friction laws and the concept of "static" friction is discussed. Measurements of frictional healing, as evidenced by increasing static friction during quasistationary contact, are reviewed, as are their implications for fault healing. Shear localization in fault gouge is discussed, and the relationship between microstructures and friction is reviewed. These data indicate differences in the behavior of bare rock surfaces as compared to shear within granular fault gouge that can be attributed to dilation within fault gouge. Physical models for the characteristic friction distance are discussed and related to the problem of scaling this parameter to seismic faults. Earthquake afterslip, its relation to laboratory friction data, and the inverse correlation between afterslip and shallow coseismic slip are discussed in the context of a model for afterslip. Recent observations of the absence of afterslip are predicted by the model.

INTRODUCTION

Since their introduction nearly 20 years ago, friction constitutive laws of the slip rate and state variable type (Dieterich 1979, Ruina 1983) have emerged as

0084-6597/98/0515-0643$08.00

powerful tools for investigating the mechanics of earthquakes and faulting. The incorporation of a state variable provided a means of describing complex friction memory effects and history dependence, and the resulting constitutive laws have been extremely successful in modeling laboratory data. These laws are capable of reproducing virtually the entire range of observed seismic and interseismic fault behaviors, ranging from preseismic slip and earthquake nucleation (Dieterich 1986, 1992, Stuart & Tullis 1995, Roy & Marone 1996, Tullis 1996, Dieterich & Kilgore 1996a) to coseismic rupture (Tse & Rice 1986, Okubo 1989, Cochard & Madariaga 1994, Ben-Zion & Rice 1995, 1997, Boatwright & Cocco 1996) and earthquake afterslip (Marone et al 1990, Wennerberg & Sharp 1997). In addition, the laws have been widely used to describe systematic variations in seismic behavior, including the depth of seismic faulting (Tse & Rice 1986, Marone & Scholz 1988, Blanpied et al 1991), variation of stress drop with earthquake recurrence interval (Scholz et al 1986, Kanamori & Allen 1986, Vidale et al 1994, Marone et al 1995), seismic slip complexity (Takashi 1992, Rice 1993, Rice & Ben-Zion 1996), variations in the stability and seismic coupling at subduction zones (Scholz 1990, Scholz & Campos 1995), and characteristics of aftershock rate decay (Dieterich 1994, Gross & Kisslinger 1997).

The past few years have seen continued growth in the application and physical understanding of friction constitutive laws. In modeling applications, improvements in the quality and spatial resolution of seismic and geodetic observations have led to significant advances in the evaluation of laboratory-based models. In the laboratory, a consensus has emerged concerning several aspects of friction data for rock and granular materials (crushed rock, sand, or powders) used to simulate fault gouge. Such studies have resolved, under a limited range of conditions, issues including the nature of frictional state evolution, the role of dilatancy and fault gouge in friction velocity dependence, and the effect of shear strain and displacement on scaling parameters and friction behavior. In addition, discrepancies between results obtained in different testing configurations are now more clearly understood.

However, in spite of their utility and widespread use, laboratory-based friction laws and their application in nature have a number of shortcomings. Chief among these are perhaps the empirical nature of the laws and the scaling problem associated with extrapolating results outside of the laboratory range of conditions. Thus, in this review, I have chosen to focus on recent laboratory results and field observations related to the scaling problem and on modeling studies aimed at applying laboratory-based laws to seismic faulting. To this end, I summarize recent results related to the rate of frictional healing, work on the effects of displacement and strain on frictional behavior, and studies of postseismic slip that can be used to infer the rheology of mature faults. For the

most part, I do not revisit topics covered in the excellent summaries of earlier reviews on this subject (Rudnicki 1980, 1988, Mavko 1981, Sibson 1986, Tullis 1988, Scholz 1989, 1990, Kanamori 1994). Yet, even with these restrictions, the topic is exceedingly broad, drawing from the detailed work of laboratory, modeling, theoretical, and observational studies. Thus, I attempt only a brief summary of progress in selected areas. Unfortunately, this rather limited scope does not encompass several fruitful lines of study, and I can only suggest a few initiation points for readers interested in works on spatio-temporal complexity and frequency-magnitude scaling of seismicity (Horowitz & Ruina 1989, Shaw et al 1992, Abercrombie & Leary 1993, Rice 1993, Wesnousky 1994, Shaw 1994, Ben-Zion & Rice 1995, Ben-Zion 1996, Sornette et al 1996, Heimpel 1996, 1997); fluid, poro-elastic, and thermal effects on friction and the seismic cycle (Mase & Smith 1987, Blanpied et al 1991, 1992, 1997, Chester & Higgs 1992, Sleep & Blanpied 1992, 1994, Chester 1994, 1995, Sleep 1994, 1995a,b, 1997, Hickman et al 1995, Segall & Rice 1995, Shaw 1995, Miller 1996, Miller et al 1996, Karner et al 1997); elasto-dynamic rupture propagation, including studies of opening mode waves and Heaton pulses (Cochard & Madariaga 1994, 1996, Perrin et al 1995, Beeler & Tullis 1996, Andrews & Ben-Zion 1997); dynamical models of earthquakes employing idealized friction laws and their connection to continuum-based models (Carlson & Langer 1989, Huang & Turcotte 1992, Carlson et al 1991, Rice 1993, Shaw 1995, Rice & Ben-Zion 1996, Schmittbuhl et al 1996, Main 1996, Rundle et al 1996); studies of granular materials and acoustic fluidization related to fault mechanics and rupture propagation (Melosh 1979, 1996, Lorig & Hobbs 1990, Mora & Place 1994, Scott 1996); studies of rupture nucleation using laboratory-derived friction laws (Dieterich 1986, 1992, 1994, Yamashita & Ohnaka 1991, Shibazaki & Matsu'ura 1992, 1995, Roy & Marone 1996, Kato & Hirasawa 1996); and laboratory and theoretical works focused on building detailed physical models of base friction using contact theory (Yoshioka & Scholz 1989a,b, Stesky & Hannan 1989, Biegel et al 1992, Boitnott et al 1992, Wang & Scholz 1994, 1995).

I begin with a brief historical introduction to the friction laws, which provides a background for understanding the significance of some important recent results concerning the nature of frictional state evolution and frictional healing. These works illuminate the relationship between so-called static and dynamic friction, terms that are dated but still of practical use, and provide a connection between laboratory observations of frictional healing and seismic estimates of the rate of fault healing. In the subsequent section, I consider the effects of fault gouge and strain on friction behavior and constitutive parameters and their implications for the scaling problem. In this case, the effects of shear localization, dilation, and net displacement are quite important. These results

are closely related to the mechanistic interpretation of the critical slip distance (defined below) and the problem of scaling this parameter to seismic faulting. A new mechanical interpretation of the critical slip distance for fault gouge is discussed in that section. Finally, application of the laboratory-derived friction laws to earthquake afterslip and the rheology of mature fault zones is reviewed. In this case, seismic data and field observations are of sufficient quality to provide constraints on laboratory-based friction laws and associated models. Because the vast majority of laboratory experiments have been carried out at room temperature and with quartzo-feldspathic materials, I focus primarily on these experiments.

FUNDAMENTALS OF LABORATORY-DERIVED FRICTION LAWS

Slip rate and state variable constitutive laws for rock friction were first introduced by Dieterich (1979, 1981), Ruina (1983), and Rice (Rice 1983, Rice & Ruina 1983). The laws were the outgrowth of a broad effort to understand rock friction, beginning in its modern form with the work of Brace and coworkers (Brace & Byerlee 1966, 1970, Byerlee 1967) and including several seminal works in the succeeding decade (Dieterich 1972, 1978, Scholz et al 1972, Ohnaka 1973, Scholz & Engelder 1976, Byerlee 1978, Logan 1978, Stesky 1978, Teufel & Logan 1978). These early works were designed to study frictional instability as a possible mechanism for repetitive stick-slip failure and the seismic cycle. The works made two primary contributions of direct relevance here. The first involved the recognition of frictional stability as a system response determined by the contacting surfaces and their elastic surroundings (e.g. Cook 1981). This led to a fundamental shift in the way laboratory studies were carried out. Simple "mapping" studies of the stability boundary between stick-slip and stable sliding were recognized as having limited value, and they were gradually replaced by more detailed studies in which friction data were subject to sophisticated modeling in order to separate stability and friction properties from apparatus effects (see Tullis 1988 for a summary). As a result, friction data were increasingly cast in terms of constitutive parameters and constitutive laws that could be readily applied in a variety of mechanical settings, including those of seismogenic faults (e.g. Dieterich 1979, 1981, Dieterich & Conrad 1984, Okubo & Dieterich 1984, Weeks & Tullis 1985, Blanpied & Tullis 1986, Lockner et al 1986, Ohnaka 1986, Shimamoto & Logan 1986, Tullis & Weeks 1986, Olsson 1988, Biegel et al 1989, Sammis & Biegel 1989, Marone et al 1990, Wong & Zhao 1990, Blanpied et al 1991, 1995, Reinen et al 1991, 1992, 1994, Chester & Higgs 1992, Linker & Dieterich 1992, Marone et al 1992, Steacy & Sammis 1992, Wong et al 1992, Kilgore et al 1993, Marone &

Kilgore 1993, Reinen & Weeks 1993, Beeler et al 1994, 1996, Chester 1994, 1995, Dieterich & Kilgore 1994, 1996a,b, Gu & Wong 1994, Kato et al 1994, Marone & Cox 1994, Sammis & Steacy 1994, Scott et al 1994, Wang & Scholz 1994, Beeler & Tullis 1997, Blanpied et al 1997, Karner et al 1997). The use of quantitative friction constitutive laws relating stress and strain or displacement also provided a context within which friction data and laboratory-based continuum models could be subject to rigorous stability analysis (Rice & Ruina 1983, Gu et al 1984, Blanpied & Tullis 1986, Horowitz 1988, Dieterich & Linker 1992).

The second contribution involved detailed measurements of the velocity dependence of sliding friction and the time dependence of static friction (Figure 1) (Dieterich 1972, 1978, 1979, 1981, Scholz et al 1972, Engelder & Scholz 1976, Scholz & Engelder 1976, Teufel & Logan 1978, Johnson 1981). These data could not be rationalized within the context of existing friction laws and required a new framework for understanding rock friction. Two aspects of these data are particularly relevant here, and I briefly summarize the original results, with recent data added where appropriate.

Figure 1*a* shows static friction measurements for granite and simulated fault gouge. The data are obtained from experiments (Figure 1*b*) in which loading and steady frictional sliding are interrupted for a specified time, here for 10 and 100 s, after which loading resumes at the original rate, a so-called slide-hold-slide test. Although the term static friction implies a measure of strength in the absence of slip, this is in fact not the case (e.g. Scholz et al 1972). Static friction μ_s is defined (Dieterich 1972) as the maximum value following a hold period, and this corresponds to the point at which slip velocity first reaches the pre-hold value. Because static friction increases with hold time, measurements of it must be carried out by first sliding and then holding so that the initiation time of the hold is known. Dieterich (1972) showed that static friction increases logarithmically with hold time, and subsequent results indicate that the rate is somewhat higher for rock than for simulated fault gouge (Figure 1*a*). These data could be fit by empirical, time-dependent strengthening laws and were consistent with creep and contact indentation models in use at that time; however, only the static friction values μ_s are fit by such laws. The laws are not capable of describing details of the time- and displacement-dependent changes in friction that accompany changes in static friction (Figure 1*b*), nor are they able to explain static friction in the context of models for velocity-dependent dynamic friction.

At the same time, measurements of dynamic friction for rock and gouge (Figure 1*c*) showed that sliding friction decreases with velocity, a phenomenon known as velocity weakening (Scholz & Engelder 1976). Early work showed that bare rock surfaces exhibited velocity-weakening friction over a range of

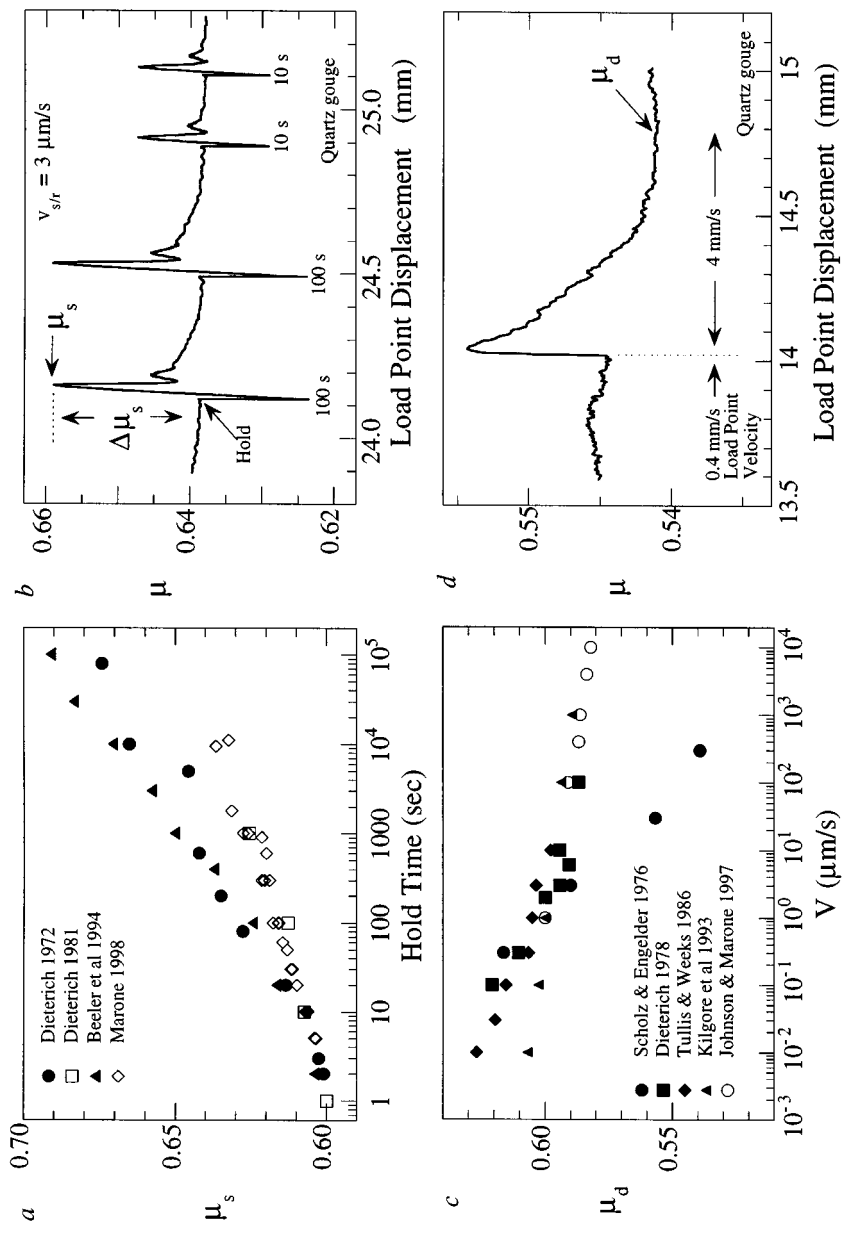
a
b
c
d
Dieterich 1972
Dieterich 1981
Beeler et al 1994
Marone 1998
Hold Time (sec)
Scholz & Engelder 1976
Dieterich 1978
Tullis & Weeks 1986
Kilgore et al 1993
Johnson & Marone 1997
V (μm/s)
$v_{s/r}$ = 3 μm/s
Hold
100 s
10 s
Quartz gouge
Load Point Displacement (mm)
0.4 mm/s
Load Point
Velocity
4 mm/s

velocities. Subsequent work indicated velocity strengthening for pervasive shear within granular gouge, with a transition to velocity weakening for localized shear, as discussed more fully below; however, for both rock and fault gouge, that data indicate that friction evolves over a finite slip distance upon a sudden change in loading velocity (Figure 1*d*). The measurements show that dynamic friction exhibits velocity weakening (i.e. μ_d decreases with increasing slip velocity) over a broad range of velocities, extending up to centimeters per second in the case of fault gouge (Figure 1*c*) and meters per second for shear of gabbro (Tsutsumi & Shimamoto 1997). In some cases at the higher velocities, friction of rock exhibits a transition to velocity strengthening (Blanpied et al 1987, Kilgore et al 1993, Weeks 1993), which is presumed to arise from the effects of frictional heating; however, such effects apparently vary with experimental configuration and other factors that remain poorly understood (Kilgore et al 1993, Spray 1993, Tsutsumi & Shimamoto 1997, Blanpied et al 1998).

A major problem posed by these observations was that of how static and dynamic friction measurements could be related. In particular, although the observations seem consistent, if hold time for static friction measurements is taken proportional to inverse average velocity, the data indicate that friction is not a single-valued function of velocity (Figure 1*d*). Thus, a simple velocity-dependent friction law is not sufficient, a point that continues to be at the root of differences between physically based and dynamical models of friction (Shaw et al 1992, Rice 1993, Myers et al 1996, Rice & Ben-Zion 1996). The other type of friction law in common use at that time, the slip-weakening law favored by those modeling dynamic shear rupture (e.g. Andrews 1976), was also insufficient because it could not describe the static friction data nor its connection to rate-dependent dynamic friction. This represented a major limitation not only to modeling laboratory data, but also to the problem of

←

Figure 1 (*a*) Measurements of the relative variation in static friction with hold time for initially bare rock surfaces (*solid symbols*) and granular fault gouge (*open symbols*). The data have been offset to $\mu_s = 0.6$ at 1 s and thus represent relative changes in static friction. (*b*) Friction data versus displacement, showing measurements of static friction and $\Delta\mu_s$ in slide-hold-slide experiments. Hold times are given below. In this case the loading velocity before and after holding $V_{s/r}$ was 3 μm/s (data from Marone 1998). (*c*) The relative dynamic coefficient of friction is shown versus slip velocity for initially bare rock surfaces (*solid symbols*) and granular fault gouge (*open symbols*). The data have been offset to $\mu_d = 0.6$ at 1 μm/s. (*d*) Data showing the transient and steady-state effect on friction (see Figure 2 for identification of friction parameters) of a change in loading velocity for a 3-mm–thick layer of quartz gouge sheared under nominally dry conditions at 25-MPa normal stress (data from J Johnson & C Marone, manuscript in preparation).

modeling repetitive stick-slip failure and the seismic cycle, which requires slip weakening to initiate unstable failure but also a healing process to reset strength between failure events.

Introduction of the rate and state friction laws resolved these problems. Static friction and its observed time dependence was revealed as a special case of velocity-dependent friction, and the full range of time and displacement-dependent variations illustrated in Figure 1 could be modeled with a single friction law. However, important differences exist in the laws introduced by Dieterich (1979) and Ruina (1983).

Friction Evolution Laws and the State Variable

Dieterich's original constitutive law (1979) stressed the importance of contact time, and thus the connection between time dependence of static friction (Figure 1*a*) and velocity dependence of sliding friction (Figure 1*c*) was via an effective contact time derived from the ratio of a critical slip distance D_c to slip velocity V. Dieterich interpreted D_c as representing the slip necessary to renew surface contacts; hence, the ratio D_c/V defined an average contact lifetime θ. This provides a connection between time and velocity dependence of friction, which may be written (using a modern form that allows easy comparison with the other laws discussed below):

$$\mu = \mu_o + a\ ln\left(\frac{V}{V_o}\right) + b\ ln\left(\frac{V_o\theta}{D_c}\right), \tag{1}$$

where μ_o is a constant appropriate for steady-state slip at velocity V_o, V is the frictional slip rate, θ is a state variable (Ruina 1983), and a and b are empirical constants. The form of Equation 1, and in particular the log terms, is suggested by the basic data of Figure 1. Dieterich's original law (1979) differed somewhat from Equation 1, in that it did not include specific reference to a state variable; however, its basic features were the same.

If the state variable θ has the interpretation of a characteristic contact lifetime, then the terms in Equation 1 scaled by the constants a and b represent ratios of velocity to a reference velocity V_o, and their summation describes the observed time and velocity dependence of friction (Figure 1). Of course, this statement omits many important details, but it includes the basic idea (Dieterich 1978, 1979) that restrengthening of friction during quasistationary contact can be accounted for with the same (state) memory effects and history dependence necessary to describe velocity dependence of steady-state sliding friction. To model details of friction arising from perturbations in average contact lifetime (state) or slip velocity, Equation 1 must be coupled with a description of state evolution:

Dieterich law

$$\mu = \mu_o + a\ ln\left(\frac{V}{V_o}\right) + b\ ln\left(\frac{V_o\theta}{D_c}\right), \qquad \frac{d\theta}{dt} = 1 - \frac{V\theta}{D_c}. \tag{2}$$

Although only the second relation (the state evolution law) in Equation 2 differs between the three rate/state friction laws discussed, I include the friction relation (Equation 1) for completeness and because the full constitutive law is defined by both relations. Also, the friction relations have been extended to include variations in normal stress (Linker & Dieterich 1992; see also Wang & Scholz 1994); however, I do not consider such effects here.

Equation 2 has been referred to as the slowness law and the Dieterich-Ruina law; however, for simplicity and to avoid confusion between laws, I refer to it simply as the Dieterich law. In this equation, state, and thus friction, evolve even for truly stationary contact with $V = 0$, which has been referred to as aging (Tullis et al 1993, Beeler et al 1994, Perrin et al 1995). It must be noted, however, that Equation 1 is undefined at $V = 0$. Although this condition is problematic for numerical computation, it is consistent with a definition of friction that is distinct from a generalized brittle shear strength or failure criteria. That is, by definition, friction is the normalized shear strength of a particular (existing) surface, and to be measured (including even static friction), the surface must undergo slip at some scale (e.g. Scholz et al 1972, Baumberger et al 1994).

Ruina (1983) proposed a different evolution law in which velocity and slip, rather than time, were of primary importance:

Ruina law

$$\mu = \mu_o + a\ ln\left(\frac{V}{V_o}\right) + b\ ln\left(\frac{V_o\theta}{D_c}\right), \qquad \frac{d\theta}{dt} = -\frac{V\theta}{D_c} ln\left(\frac{V\theta}{D_c}\right), \tag{3}$$

where it is understood that the full constitutive law is defined by both parts of Equation 3 (the symbols have been defined above). In this view, the importance of truly stationary contact for static friction and strength recovery is discounted, and the connection between time dependence of static friction and velocity dependence of sliding friction is via an effective velocity derived from the ratio of D_c to the time of quasistationary contact.

Thus, while Dieterich's model casts friction primarily in terms of time dependence and static friction, Ruina's model takes the opposite view, such that any change in friction, including strengthening during quasistationary contact, requires slip. In particular, Ruina used data showing that friction exhibits memory effects, in the form of a critical slip distance required to effect a change from one value to another (Rabinowicz 1951, 1958), and precursive slip prior to unstable failure (Scholz et al 1972) to argue that all changes in friction involve slip. Time dependence of static friction, in this view, is due to slip occurring

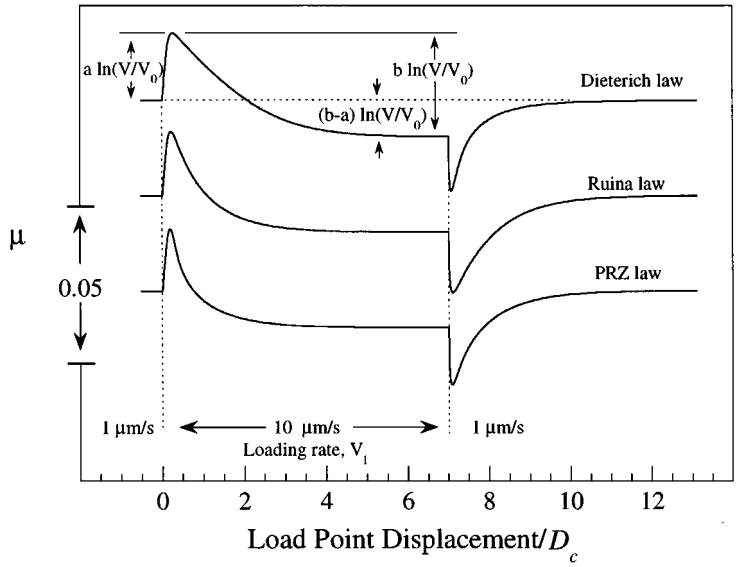

Figure 2 Friction versus normalized displacement is shown for the three rate and state friction laws discussed. Constitutive parameters are defined at the top and apply to each *curve*. The effect of a step increase and decrease in load point velocity is shown for each law using the parameters given. $V_o = 1$ μm/s. The *curves* were calculated for the following parameters: $a = 0.01$, $b = 0.015$, $D_c = 20$ μm, and $k = 0.01$ μm^{-1}.

during the hold period, and this is not inconsistent with the observations, since the stress reduction during holding (Figure 1*b*) results from slip.

Although the distinction between the two views of friction evolution is fundamental in terms of micromechanical interpretation of the underlying processes, the laws reproduce laboratory data in a similar fashion (Figure 2). That is, in each case a longer-term evolution process, which leads to velocity weakening in some cases (Figure 1*c*), competes with a shorter-term "direct effect," in which friction increases for an increase in load point velocity and decreases upon a decrease in velocity (Dieterich 1979). The laws differ in their predicted responses to step increases and decreases of velocity (Figure 2). In Dieterich's law, because of the importance of effective contact time, the slip necessary for friction to regain a steady state following a perturbation scales with velocity, and thus the friction displacement curves for velocity changes of opposite sign are asymmetric (Figure 2). In contrast, the approach to a steady state is independent of time and thus symmetric with respect to velocity changes for Ruina's law. A third law has been proposed recently by Perrin, Rice, and Zheng (Perrin et al 1995). Their law exhibits both aging and symmetry with respect

to velocity changes:

PRZ law

$$\mu = \mu_o + a\ ln\left(\frac{V}{V_o}\right) + b\ ln\left(\frac{V_o\theta}{2D_c}\right), \qquad \frac{d\theta}{dt} = 1 - \left(\frac{V\theta}{2D_c}\right)^2. \tag{4}$$

This law yields a response similar to that of the others (Figure 2), with the decay to steady state for a linearized perturbation proportional to $\exp(-u/D_c)$, where u is slip. For steady-state sliding, each of the laws gives

$$(a - b) = d\mu_{ss}/dln(V), \tag{5}$$

and thus the slope μ_d versus V on Figure 1*c* is given by $(b - a)ln(10)$.

To model variations in frictional strength, the constitutive law must be coupled with a description of elastic interaction between the frictional surfaces and their surroundings. Tullis (1988) reviewed several key aspects of such modeling and showed the relationship between laboratory data and predictions based on stability analyses. In laboratory experiments, single-degree-of-freedom elastic coupling is generally sufficient:

$$d\mu/dt = k(V_l - V), \tag{6}$$

where V_l is the velocity of a load point, inertia is taken to be negligible, and the frictional surface is assumed to be rigid so that all elastic deformation is accounted for by the spring constant k of the testing machine, here expressed as the ratio of elastic stiffness to normal stress.

Which State Evolution Law?

The question of which law best describes friction evolution in the laboratory and for seismogenic faults is of great interest because despite their apparent similarity (Figure 2), the different evolution laws yield qualitatively different behavior in simulations of seismic phenomena (Horowitz & Ruina 1989, Rice 1993, Perrin et al 1995, Beeler & Tullis 1996, Wennerberg & Sharp 1997). A common theme derived from these works is that friction laws that exhibit true aging are, under some conditions, required to reproduce certain features of dynamic faulting, including Gutenberg-Richter–like frequency-magnitude statistics (Rice 1993) and slip-pulse rupture propagation (Heaton 1990, Perrin et al 1995, Beeler & Tullis 1996). Unfortunately, distinguishing between the laws in the laboratory, even at room temperature, has proven difficult. The symmetry of velocity changes has not provided a robust means of distinguishing between the laws. Early experiments seemed to find in favor of Ruina's law (Ruina 1983, Tullis & Weeks 1986, Marone et al 1990), and recent work on the effect of normal stress indicates that state evolution may be more closely related to slip than time (Linker & Dieterich 1992); however, the distinction is

subtle and often unresolvable owing to noise and other trends in the data. This is particularly true for studies focusing on perturbations around steady state (Tullis et al 1993).

An obvious test to distinguish between the Dieterich and Ruina evolution laws would be to completely remove the shear load during holds when measuring static friction. In this case, no slip would occur during the hold period, and thus the Ruina law predicts no change in θ or μ, in contrast to predictions of an aging law. However, conducting such an experiment is difficult because the shear load must be removed and reapplied quickly, without reversal, and the surfaces must be held in position to within a fraction of D_c. A few studies have been done in which shear load is partially removed and held constant during holds (e.g. Nakatani & Mochizuki 1996), and these show that the relative change in static friction, $\Delta\mu_s = \mu_s - \mu_o$, scales inversely with the magnitude of the shear load reduction.

However, an alternative approach has produced the most promising results to date (Beeler et al 1994). Beeler and coworkers recognized that by varying the effective stiffness of their testing machine, they could independently control the slip and time during a slide-hold-slide test (Figure 1*b*). They conducted experiments using the natural stiffness k_n of their testing machine and an artificially higher stiffness ($k_s > k_n$) produced by servocontrol, in which the displacement of a load point, rather than the force, is controlled, resulting in an artificially high stiffness. Their data are reproduced in Figure 3. The measurements of $\Delta\mu_s$ as a function of hold time show that the healing rate ($\beta = \Delta\mu_s$ per decade change in hold time) is independent of stiffness (Figure 3). By comparing their results with predictions of the constitutive laws, they were able to show conclusively that their data obey an aging law, such as that of Dieterich.

Two aspects of Beeler et al's (1994) data and analysis are of particular interest. First, within the scatter in the data, they observed that both the absolute values of healing and the healing rate are identical for the experiments at high and low stiffness. Numerical simulations using the Dieterich law and a given loading velocity ($V_{s/r}$, see Figure 1*b*) show that β is not a function of stiffness at long hold times, but that the absolute values of $\Delta\mu_s$ vary directly with stiffness (Figure 3; Beeler et al 1994). This is consistent with the form of Equation 3, which specifies a competition between time (which causes strengthening) and slip (which reduces strength), since a smaller amount of slip occurs during a given hold for the higher stiffness. On the other hand, Ruina's law predicts that both $\Delta\mu_s$ and β decrease with increasing stiffness; hence, a more compliant system would yield greater static frictional strength for a given hold time. Beeler et al (1994) focused primarily on the healing rate and showed numerical simulations of the friction law calculated for a single $V_{s/r}$. However, their experiments were conducted at different velocities: $V_{s/r}$ was 1.0 and 0.3162 μm/s for k_n and k_s, respectively.

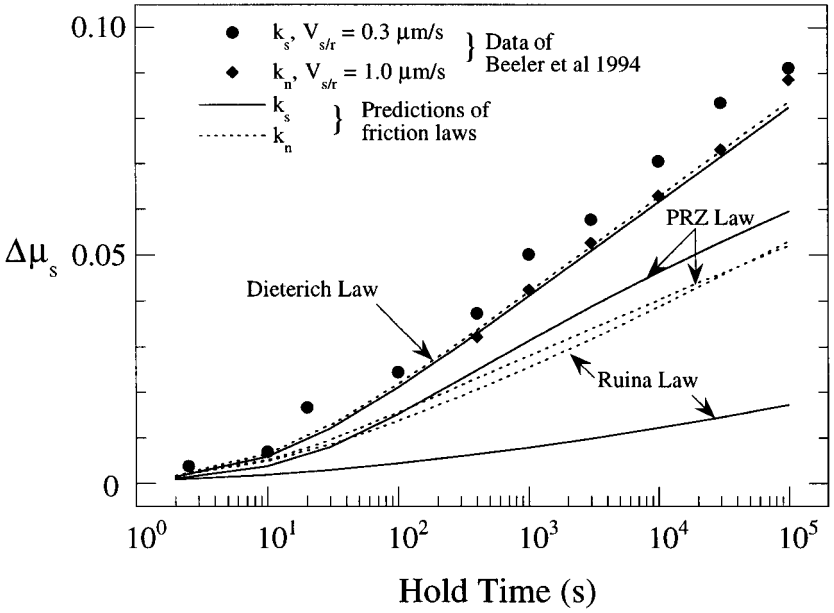

Figure 3 Time dependence of the change in static friction (see Figure 1*b*) for initially bare granite surfaces, as measured for two stiffnesses of the testing apparatus $k_n = 0.002\ \mu\text{m}^{-1}$ and $k_s = 0.074\ \mu\text{m}^{-1}$, expressed as stiffness normalized by normal stress (data from Beeler et al 1994). Also shown are predictions of the rate and state friction laws computed using the stiffnesses and loading velocities $V_{s/r}$ given and the following friction constitutive values, as reported by Beeler et al (1994): $a = 0.008$, $b = 0.009$, $D_c = 3.0\ \mu$m. (Figure modified from Beeler et al 1994.)

In Figure 3, I show numerical simulations using Beeler et al's (1994) experimental conditions and actual loading velocities for k_n and k_s. The comparison shows that for the Dieterich law, both the absolute values of $\Delta\mu_s$ and the healing rate are the same, as indicated by their data. Thus, agreement between their data and predictions of the Dieterich law is improved by accounting for the actual velocities. On the other hand, this accounting enhances difference between the Ruina law predictions for k_n and k_s and thus moves these further from the experimental observations. The PRZ law shows a smaller effect of stiffness and loading velocity compared with the Ruina law; however, the predicted values of $\Delta\mu_s$ and healing rate do not match the observations (Figure 3).

Thus, the data of Beeler et al (1994) indicate that rock friction evolves even during truly stationary contact, at least for the conditions of their study. This is consistent with mechanistic interpretations in which the real area of surface contact increases with time, owing to interpenetration and/or creep (Dieterich 1978, Dieterich & Conrad 1984, Kato et al 1993). However, the generality

of this conclusion as applied to other conditions of temperature and chemical environment remains to be tested, as does the connection between healing measurements and the behavior observed for velocity perturbations.

LABORATORY AND FIELD OBSERVATIONS OF FRICTIONAL HEALING

A straightforward extension of the healing data and modeling results discussed above indicates that static friction and the rate of frictional restrengthening during quasistationary contact vary with loading rate. This has an interesting implication for the application of laboratory friction data to the problem of fault healing. In addition, it implies that the simple connection often assumed between variations in static and dynamic friction is flawed. In this section, I briefly outline these issues, drawing from recent laboratory results and field estimates of fault healing.

The Rate of Frictional Healing

Figure 4 shows data from experiments similar to those illustrated in Figures 1 and 3, in which static friction was measured for a range of hold times (Marone 1998). In these experiments, layers of granular quartz powder were sheared within rough granite surfaces at 25-MPa normal stress, but unlike the techniques used for Figure 3, the same apparatus stiffness was used for each set of tests. The data show that static friction and time-dependent healing $\Delta\mu_s$ vary systematically with loading rate. Related effects have been demonstrated by Johnson (1981) and Kato et al (1992), as well as by the data of Beeler et al (1994), as discussed above.

The data of Figure 4 have two important implications. First, they indicate that laboratory measurements of static friction and time-dependent healing must be scaled appropriately for comparison with seismic estimates of fault healing. That is, the data show that frictional healing is a system response and thus, like measurements of velocity-dependent friction, must be subject to modeling in order to recover the governing constitutive parameters (Marone 1998). The constitutive parameters may be used in applying the results to different conditions; however, without such modeling, the static friction values are strictly applicable only to the particular laboratory-testing machine with which they were measured.

Second, the observation of a loading rate effect on static friction (Figure 4) indicates that the healing mechanism is not just a function of time. The observations indicate that $\Delta\mu_s$ varies approximately as the product of loading rate and hold time, which implies that the mechanism of frictional strengthening is a function of slip and time. This is a feature of the rate and state friction

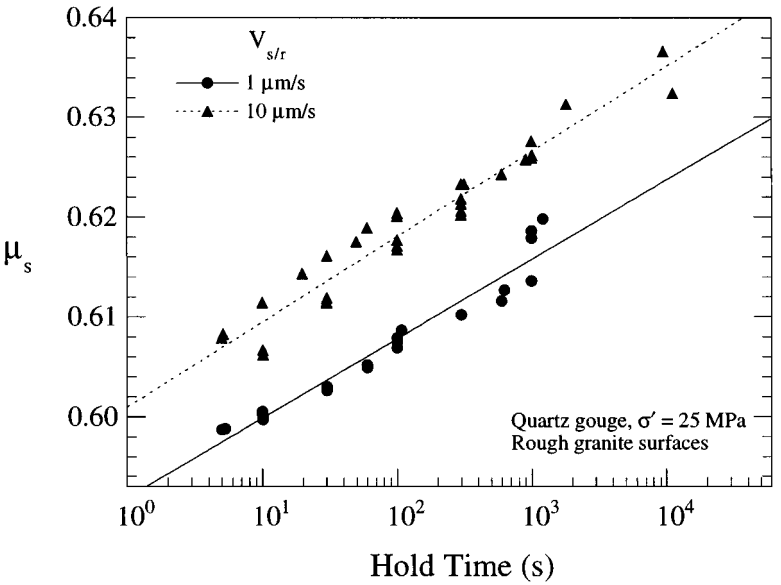

Figure 4 Time dependence of static friction for loading with $V_{s/r} = 1$ and 10 μm/s. The data indicate that static friction and healing vary with loading rate and therefore that static friction is a system response. *Lines* represent best fit log-linear relations. (Figure from Marone 1998.)

laws, and indeed, when combined with a description of elastic interaction such as Equation 6, the laws show that for a given set of constitutive parameters, $\Delta\mu_s$ increases with loading velocity, as is observed. However, the cause of this effect is complex. It is not simply an effect of the second term in Equation 1, the so-called direct effect, as would be implied by replacing V in this equation with $V_{s/r}$. That is, slide-hold-slide tests measure relative changes in friction, and thus to compare tests conducted at different velocities, the term V_o in Equation 1 must also be changed. Moreover, because of the way static friction tests are carried out, the a term of Equation 1 is zero when static friction is measured. This can be seen by noting (Figure 1*b*) that static friction is a local maximum and thus a point at which $\Delta\mu_s/dt = 0$, which from Equation 6 indicates that surface slip velocity equals loading velocity. However, the direct effect term is important because it moderates the amount of slip that occurs during a hold and thus influences the amount by which the frictional state changes (Marone 1998).

These points have two important implications when coupled with the results of Beeler et al (1994), showing that healing exhibits Dieterich-law–style aging. First, since slip velocity approaches zero in the limit of long hold time, from

Equation 2 with $d\theta/dt = 1$ in the limit, frictional healing rate is given by $b\ ln(t)$. Thus the healing rate for long holds should scale as b, as noted by Beeler et al (1994). Second, the influence of loading velocity on healing rate must enter through an effect on state θ. This is confirmed by modeling, which shows that for larger initial values of $V_{s/r}$, surface slip velocity decreases faster during the initial time increments of the hold, and V reaches lower values in a given time (Marone 1998). From the Dieterich evolution law, lower V results in a higher value of state, which yields larger values of $\Delta\mu_s$.

Although rate and state friction laws are capable of describing complex behavior such as velocity-dependent healing, most laboratory studies of healing have considered only a single loading rate. Also, systematic measurements have tended to be restricted to static friction, without reference to other features of the data, such as the minimum friction reached at the end of the hold. Careful attention to such factors offers the possibility of providing further tests of the friction laws and possibly additional constraints on frictional behavior (e.g. Karner et al 1997).

The Rate of Fault Healing

Laboratory friction measurements at room temperature and for the conditions expected in the nucleation region of large earthquakes (Karner et al 1997) show that frictional healing proceeds linearly with log time during quasistationary contact. This is consistent with seismic estimates of fault healing (Kanamori & Allen 1986, Scholz et al 1986, Vidale et al 1994, Marone et al 1995), which also show an approximately log-linear strengthening rate. However, as pointed out originally by Scholz et al (1986) and Cao & Aki (1986), there is a large apparent discrepancy in the rates. Rock friction increases by only a few percent of its absolute value per decade in time (Figure 1), whereas seismic stress drop increases by a factor of 2–5 per decade increase in earthquake recurrence interval.

A number of possible explanations for this discrepancy have been suggested (Scholz 1990, Marone et al 1995). For example, differences in the time scale and chemical conditions of laboratory samples and tectonic faults have been noted (Scholz 1990, Wong & Zhao 1990). Also, Scholz (1990) discussed several explanations relating to differences in the frictional properties of faults from different tectonic regimes and with different slip rates and total offsets. However, the work of Vidale et al (1994) and Marone et al (1995) on earthquakes that repeatedly rupture the same fault patch showed roughly the same healing rate as that inferred from different faults; therefore this explanation is not likely. Rather, as suggested by Marone et al (1995), the discrepancy may arise from differences in the way healing rate is measured in the lab and from seismic data.

In laboratory studies of frictional healing, small changes are observed in the absolute value of friction as a function of hold time. The changes are but a few percent of the nominal friction value. For example, μ is $\sim$0.6 and the healing rate is $\sim$0.01 per decade change in hold time, expressed as a coefficient of friction (Figure 4). As applied to earthquake rupture and seismic stress drop, the healing data indicate that static frictional yield strength would vary by the same amount, say 1 MPa per decade for a fault under a normal stress of 100 MPa. For our nominal friction value, shear strength of this fault would be 60 MPa. Thus if earthquake stress drop $\Delta\sigma$ were complete, such that $\Delta\sigma = \sigma_o - \sigma_f$ (where σ_o is initial stress, which must equal the static frictional yield strength in the initiation region) and σ_f is the final stress, given by dynamic frictional strength (which must be zero for complete stress drop), then the friction healing data indicate a negligible change in stress drop. For a factor of 10 increase in waiting time between events, stress drop would increase by only about 2%. On the other hand, if stress drop is a fraction of the total strength, such as expected on the basis of laboratory friction data (e.g. Scholz 1989, 1990, but see also Byerlee 1990, Hickman 1991, Rice 1992, and Beroza & Zoback 1993 for a fuller discussion of these issues), healing would result in a larger effect on stress drop. Moreover, if, instead of focusing on the percentage change in stress drop and frictional yield strength, the expected absolute changes in $\Delta\sigma$ are compared, then the discrepancy essentially vanishes. That is, from the above example, the frictional healing data indicate a change of stress drop of about 1 MPa per decade increase in waiting time between events. This is actually rather close to the average values reported from scaling relations (Scholz 1990) and repeating earthquakes (Marone et al 1995). The estimate from repeating earthquakes was 1–3 MPa per decade. Of course, the value given here from laboratory data would be reduced if fault normal stress were lower. Also, the healing rate used came from room temperature experiments, whereas higher values are indicated from work using more realistic conditions (Fredrich & Evans 1992, Karner et al 1997). Thus, from the available field and laboratory observations, the discrepancy in healing rate is not great.

Implications for the Relationship Between Static and Dynamic Friction

Rate and state constitutive laws specify a continuum of friction values as a function of slip rate and evolving surface state. However, owing to their historical significance and everyday relevance, the terms static and dynamic friction remain in common use. As a result, simple relationships between them are often sought, and in particular the connection between time-dependent changes in static friction and velocity-dependent changes in dynamic friction has been of significant interest. A typical assumption is that variations in static friction

can be related to variations in dynamic friction by casting the time of static contact as an average velocity, using D_c or another characteristic length scale (e.g. Scholz 1990). A similar assumption is made implicitly by Cao & Aki (1986) in their analysis of fault healing. However, these assumptions are incorrect and lead to misinterpretations when applied to laboratory and seismic data.

From the data shown in Figure 4 and associated discussions, the variation of static friction with hold time is $d\mu_s/dt \sim b\,ln(t)$ for long hold times. On the other hand, from the definition of the friction rate parameter, dynamic friction varies as $d\mu_d/dlnV = a - b$. Variations in μ_s and μ_d may be compared by plotting static friction versus inverse time and dynamic friction versus velocity. Figure 5 shows such a plot using the data for quartz gouge from Figures 1*b* and 4. Hold time and velocity are nondimensionalized, and the data are offset for comparison so that dynamic friction at 1 μm/s $= 0.6$ and static friction $= 0.6$ for $V_{s/r} = 10$ μm/s and $t_h = 1$ s. As expected, the static and dynamic friction data show different slopes because static friction scales as b, whereas dynamic friction scales as $b - a$ (Figure 5). Moreover, the offset in static friction due to

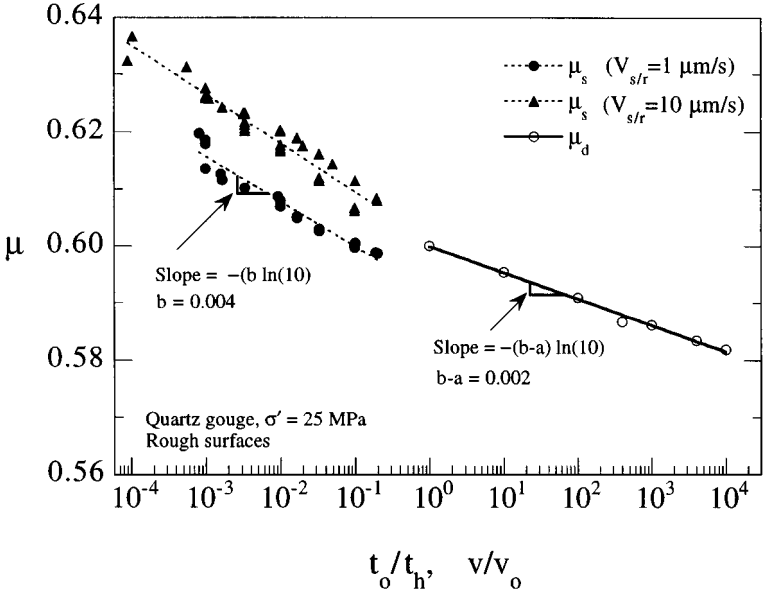

Figure 5 Static and dynamic friction are shown versus nondimensional velocity and inverse nondimensional time. The data sets are each from experiments on quartz fault gouge and indicate different slopes for static and dynamic friction, as expected from analysis of the rate and state friction laws. The inconsistency in *slope* indicates that variations in dynamic and static friction are not related through a simple scaling of static hold time as an average velocity, as is often assumed. Data are the same as those in Figure 1*c* and Figure 4.

$V_{s/r}$ illustrates the problem of using such data without accounting for the effect of loading velocity.

Scholz (1990) made a plot similar to Figure 5 (his figure 2.18) using friction measurements for different materials and found consistent trends across the data sets of static and dynamic friction, in contrast to the result given here. He plotted both types of data versus velocity by normalizing hold time for static friction measurements by the characteristic friction distance D_c. However, the effect of this normalization is only an offset of the data, and thus this cannot explain the differences in comparison with Figure 5. Rather, it is likely that subtle differences in the friction constitutive parameters of the different data sets used, due to displacement-dependent effects or differences in materials, result in a fortuitous correlation. Such effects are discussed in the following section, although in a somewhat different context.

EFFECTS OF DISPLACEMENT AND SHEAR LOCALIZATION ON CONSTITUTIVE PROPERTIES OF ROCK AND SIMULATED FAULT GOUGE

A central goal of laboratory and theoretical studies of rock friction has been to identify the mechanical conditions and constitutive properties that distinguish stable from unstable sliding. In the context of rate and state friction laws, stability analyses show that this distinction is governed by the friction rate parameter $a - b$ and the critical slip distance D_c (Rice 1983, Rice & Ruina 1983, Gu et al 1984), with potentially unstable sliding for $a - b \leq 0$ and inherently stable slip otherwise. Thus, a major preoccupation of laboratory experimentalists for the past decade or so has been to determine these friction parameters for a range of conditions, with the hope that key processes can be identified and appropriate scaling relations can be derived to connect the laboratory data with field observations. In this section, I summarize recent work in this area, with particular focus on the role of fault gouge and dilatancy and the effects of shear displacement, strain, and shear zone dimensions.

The Scaling Problem

Many aspects of laboratory friction experiments are highly idealized relative to natural faults, and at first glance it is not at all clear that results from laboratory-sized samples can provide information relevant to earthquake faulting. However, despite significant differences in fault dimensions and other factors, it is well established that the first-order aspects of shallow earthquakes are reproduced in laboratory experiments, including observations of aseismic creep, earthquake-like instability, and the transition to dominantly stable deformation as a function of increasing temperature (e.g. Scholz 1990). Other similarities

and examples have been noted in the above discussion, and of those, the similarity between laboratory and seismic estimates of the fault healing rate may be highlighted. The explanation for this apparent utility is presumed to derive from the nondimensional nature of the coefficient of friction and perhaps from self-similarity of earthquake rupture processes with respect to scale. However, nondimensionality extends only to the strength terms that give rise to friction, whereas slip stability depends on both variations in strength and on the slip distance over which these variations occur. Thus, while it is expected that some general aspects of friction can be applied more or less directly from the laboratory to field conditions (Raleigh et al 1976, Byerlee 1978), details related to slip stability must be scaled appropriately. As applied to rate and state friction laws, this implies that the nondimensional rate parameters a and b may be used directly but that the critical slip distance must be scaled; a conjecture that is supported by the available modeling studies and field-based estimates of friction parameters (e.g. Tse & Rice 1986, Scholz 1988a, Lorenzetti & Tullis 1989, Marone et al 1991, Dieterich 1992, Power & Tullis 1992, Marone & Kilgore 1993, Rice 1993, Dieterich 1994, Dieterich & Kilgore 1996a, Tullis 1996, Ben-Zion & Rice 1997, Marone 1998).

A second aspect of the scaling problem involves the effects of displacement, strain, and fault zone structure on the friction rate parameter $a - b$. Like the issues related to D_c and its scaling, the fundamental problem here involves a practical limitation. That is, laboratory experiments cannot reproduce the total displacements (10^2–10^3 m) nor roughnesses of mature fault zones, which in turn means that factors deriving from displacement and roughness, such as wear and fault zone width, shear localization, and development of microstructures, must be studied independently. However, for understanding the application in nature of laboratory measurements of $a - b$, the approach has been different and somewhat more contentious with regard to assessment of different results, as discussed below.

Finally, a much broader view of the scaling problem may be taken, with inclusion of factors such as rock type, the presence and chemistry of fluids, and extrinsic variables such as temperature, pressure, and strain rates. However, these are for the most part accessible as laboratory control variables and hence, with proper knowledge of fault zone properties and geometry, could be studied directly. Thus I do not consider such factors here.

Fault Gouge and the Second-Order Nature of Friction Rate Dependence

Early laboratory friction studies (Byerlee 1967) and observations of natural and experimentally produced fault zones (Engelder et al 1975, Logan et al 1979, Rutter et al 1986, Chester & Logan 1987, Marone & Scholz 1989, Chester

et al 1993, Beeler et al 1996) indicate that one of the most important scaling factors involves the presence and internal structure of fault gouge. Byerlee's (1967) original work showed that the accumulation of fault gouge tended to stabilize slip relative to shear between bare rock surfaces, and subsequent work, in which crushed rock and other materials were introduced to simulate fault gouge (Engelder et al 1975), confirmed this result. The connection between these two observations involves wear, as discussed by Scholz (1987) and Power et al (1988). Recently, Wong et al (1992) experimentally demonstrated the stabilizing effects of wear. These studies indicate that gouge zones widen and friction behavior evolves with accumulated displacement, which illustrates that laboratory friction results must be scaled to account for fault gouge and cumulative slip when applied in nature.

However, in most cases, the effect of fault gouge and the variations in friction velocity dependence are quite subtle (Figure 6). Dieterich & Kilgore (1994), in a detailed study of the relationship between frictional behavior and surface contact properties, observed that the effect of granite fault gouge on the friction rate parameter was quite small compared to rate-dependent effects observed for other materials. Their data show that initially bare granite surfaces exhibit approximately the same steady-state friction rate dependence as granite separated by a thick (1 mm) layer of crushed granite fault gouge (for highly localized shear at the rock boundary, as discussed more fully below), with friction parameter a approximately equal to b in each case. A much greater effect is observed for D_c, which is significantly larger for the case involving gouge (Figure 6). Moreover, their observations indicate similarity in the behavior of a wide range of materials, which involve different friction deformation mechanisms, and thus imply broad applicability of the rate and state friction formalism (Dieterich & Kilgore 1994, 1996a).

Friction parameters are known to vary with shear displacement (Dieterich 1981), and thus differences in slip may explain part of the similarity in $a - b$ for shear with and without fault gouge, as shown in Figure 6. Nevertheless, the fact that such similarity in behavior is observed for materials sheared in the same experimental configuration indicates that it is not surprising that different investigators have found slightly dissimilar results regarding friction velocity dependence (Dieterich 1979, 1981, Johnson 1981, Solberg & Byerlee 1984, Lockner et al 1986, Morrow et al 1986, Tullis & Weeks 1986, Blanpied et al 1987, 1991, 1995, Marone & Scholz 1988, Tullis 1988, Biegel et al 1989, Morrow & Byerlee 1989, Marone et al 1990, Wong & Zhao 1990, Wong et al 1992, Kilgore et al 1993, Beeler et al 1996). These works all include experiments conducted at room temperature and with quartzo-feldspathic materials, yet they employ slightly different experimental conditions and testing configurations; some investigators observe velocity strengthening, and others velocity weakening

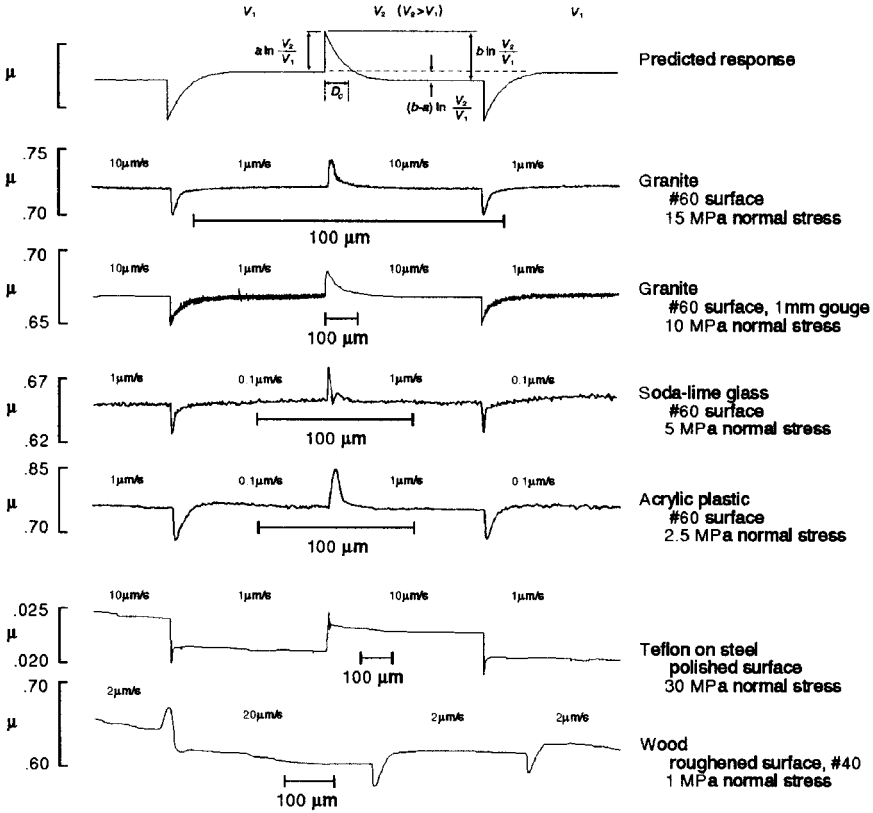

Figure 6 Friction behavior for a wide range of materials is shown for step changes in load point velocity (Dieterich & Kilgore 1994). The predicted response is that given by the rate and state friction laws. The data show remarkable similarity, indicating wide applicability of the rate and state friction formalism.

of varying degree. There has been concern that apparatus effects such as differences in sample geometry and jacketing materials were the cause of such variations (see Tullis & Weeks 1986 for a discussion). However, careful analysis of such effects and comparison of data for identical materials using different experimental geometries suggests that this is not the primary cause (Marone et al 1990; personal communications from JD Byerlee, JH Dieterich, and TE Tullis). Instead, as indicated by Figure 6, differences in reported behaviors are likely the result of interplay between a combination of subtle effects, involving differences in displacement at which data were compared, gouge layer thickness, surface roughness, normal stress, slip velocity, and perhaps material (for example, pure quartz versus crushed granite).

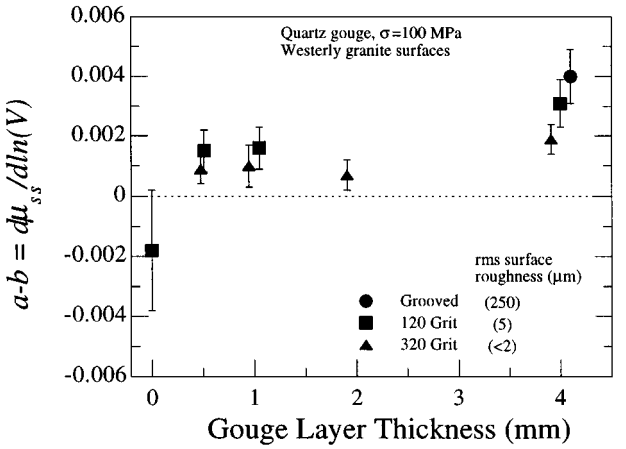

Figure 7 The friction rate parameter is shown for a series of experiments in which different initial thicknesses of quartz gouge were sheared within granite surfaces at a normal stress of 100 MPa. Bare rock surfaces show negative $a - b$ and therefore velocity weakening, whereas velocity strengthening is observed for thicker layers. The degree of velocity strengthening increases with layer thickness and surface roughness. The data are from the same shear displacement range in each experiment and thus represent different average shear strains within the gouge. (Figure and data from Marone et al 1990.)

This interpretation is supported by similarities in other friction characteristics among different investigations and data showing reproducible, systematic effects for a given set of conditions. For example, the observation that gouge accumulation tended to stabilize slip during shear of initially bare surfaces was made using a number of different experimental configurations (Byerlee 1967, Scholz et al 1972, Engelder et al 1975). Moreover, Byerlee & Summers (1976) observed that the degree of stabilization increased with gouge layer thickness, which is exactly the same conclusion to be drawn from the data of Marone et al (1990), who found a positive correlation between friction rate dependence and gouge layer thickness (Figure 7). The data of Figure 7 show velocity weakening for initially bare granite surfaces and velocity strengthening of increasing magnitude for shear of thicker gouge layers and rougher surfaces. Thus, while the initial observations of the stabilizing effect of fault gouge (Byerlee & Summers 1976) were consistent with either increased D_c or more positive $a - b$, the results of Marone et al (1990) indicate that the change in friction rate dependence ($a - b$) is the most likely cause.

The systematic variation in the friction rate parameter as a function of gouge thickness and roughness (Figure 7) is also consistent with detailed studies showing a reduction in $a - b$ and a transition to velocity weakening as a function of shear displacement. Figure 8 shows data from a number of different

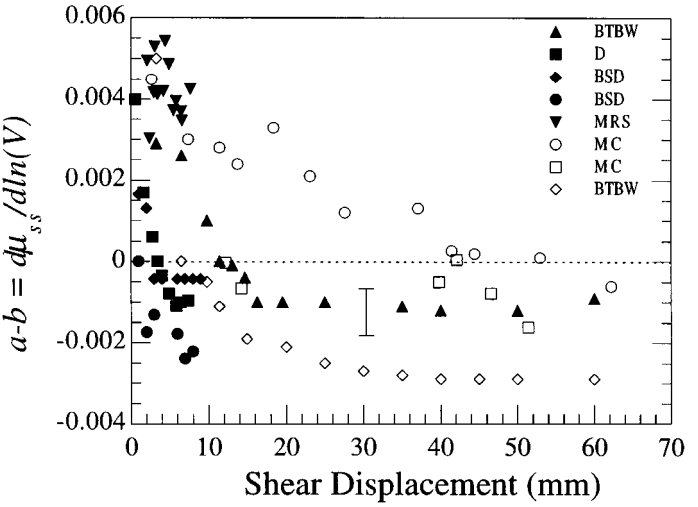

Figure 8 Variations in the friction rate parameter with shear displacement are shown for a range of materials and experimental testing configurations. The data sets indicate a transition from velocity strengthening, initially, to velocity weakening with displacement. The transition displacement varies with surface roughness and gouge layer thickness. *Error bar* shows typical experimental uncertainty. Data are indicated as BTBW (Beeler et al 1996), D (Dieterich 1981), BSD (Biegel et al 1989), MRS (Marone et al 1990), and MC (Marone & Cox 1994). The experimental conditions are as follows: For BTBW, *solid triangles* are 1-mm thick layers of granite gouge sheared within #60 grit surfaces at a normal stress of 25 MPa, and *open diamonds* are bare granite, #60 grit surfaces, 25 MPa; for D, 1-mm granite gouge, #60 grit surfaces, 10 MPa; for BSD, *solid circles* are 3-mm granite gouge, #600 grit surfaces, 10 MPa; for MRS, 4-mm quartz gouge, grooved (extremely rough) surfaces, 100 MPa; for MC, *open circles* are bare gabbro, sandblasted surfaces, 5 MPa; and for MC, *open squares* are bare gabbro, #60 grit surfaces, 5 MPa.

investigations for shear with and without fault gouge, including data for friction of gabbro and granite surfaces. Many of the data sets involve limited net slip; however, a consistent observation from these data and from the large-displacement experiments done in rotary shear with gouge (Beeler et al 1996) is that the friction rate parameter decreases with displacement and becomes velocity weakening. Several systematic effects are apparent in these data (Figure 8). 1. The transition distance from velocity-strengthening to velocity-weakening D_t increases with surface roughness (Biegel et al 1989, Marone & Cox 1994, Marone 1995). 2. For a given surface roughness, D_t is larger for experiments with an initial gouge layer compared with initially bare surfaces (Marone et al 1990, Beeler et al 1996). 3. D_t increases with initial gouge particle size (Biegel et al 1989, Marone 1993). 4. For the relatively smooth surfaces produced by polishing with #60 grit [root-mean-square (rms) roughness of $\sim$10 μm], D_t

is consistently in the range of 5–10 mm (Figure 8). Finally, for the range of displacements over which data can be compared from different experimental configurations, shear of initially bare granite and gabbro surfaces and shear of thick granite fault gouge show roughly the same degree of velocity weakening. However, as discussed below, for even larger displacements, the work of Beeler et al (1996) shows a transition back to velocity strengthening for gouge.

One feature of these data that is not well explained in the context of early friction data is the consistent observation of velocity weakening (Beeler et al 1996), for initially bare granite surfaces. The observations of Byerlee (1967) and others would imply initial velocity weakening and a transition to velocity strengthening as a function of slip. However, the early experiments were done in a triaxial configuration, and thus net shear displacements were limited to only a few millimeters. In this range, the rotary shear experiments show both velocity strengthening and velocity weakening (Beeler et al 1996). The triaxial experiments were done at much higher normal stresses (100 MPa and higher) and in some cases with larger surface roughness than the experiments of Beeler et al (1996), and thus one possible explanation for the discrepancy is that a thicker gouge layer accumulated initially due to a larger wear rate (Power et al 1988). This conjecture is consistent with the results of Tullis & Weeks (1986), who found that $a - b$ increased with slip in their rotary shear experiments at higher normal stresses (27–84 MPa), and with those of Wong et al (1992), who reported stabilization of faulting by cumulative slip at normal stresses of 100–200 MPa. However, the data necessary to fully understand the effects of wear on friction rate dependence are not available. Nevertheless many experiments done in the triaxial geometry with simulated fault gouge (Byerlee & Summers 1976, Shimamoto & Logan 1981) show a transition to unstable behavior with increasing displacement, which is consistent with a transition to velocity weakening due to the effects of shear localization as discussed below.

Scaling of Laboratory Friction Data to Natural Faults

The data of Figures 7 and 8 indicate that shear within thick gouge layers exhibits velocity-strengthening frictional behavior, but with sufficient displacement, a transition occurs to velocity weakening. Thus these data have two possible interpretations with respect to their application to crustal faults. First, since mature faults have typically undergone very large displacements relative to the laboratory scale, one could simply assume that the behavior at larger displacement is most applicable. On the other hand, since mature faults are many orders of magnitude wider and rougher than experimental fault zones and involve significantly higher wear rates, perhaps the initial behavior of laboratory

experiments on thick gouge layers sheared within rough surfaces is most applicable. In the first interpretation, the underlying cause of velocity strengthening and the transition to weakening is irrelevant for mature faults, whereas in the second, this distinction defines a stability transition that should be associated with a change from aseismic to seismic faulting (Marone & Scholz 1988). If the restriction of considering only mature faults is relaxed, then the stability transition associated with the displacement D_t may have application to variations in the seismic behavior of faults as a function of cumulative offset (e.g. Wesnousky 1988, 1990). Also, the transition from velocity strengthening to velocity weakening may have implications for the depth dependence of fault rheology. Before further discussion on these points, I consider the questions of why gouge exhibits (*a*) velocity strengthening under any conditions and (*b*) a transition to velocity weakening.

The Role of Dilatancy in Producing Velocity Strengthening in Granular Fault Gouge

It is clear from the early friction studies that the presence of gouge has an important effect on frictional stability (Engelder et al 1975, Byerlee & Summers 1976, Shimamoto & Logan 1981). These investigators recognized the possible relationship between instability and porosity changes (Edmond & Paterson 1972, Weeks & Byerlee 1978); however, for the most part they did not have the benefit of servocontrol technology and high-precision equipment, and thus they were unable to carry out detailed friction measurements in which volumetric strain within the gouge layer was measured during shear. Also, many of the initial experiments were carried out in the standard triaxial geometry, for which confining pressure is held approximately constant during loading, and thus measurements of porosity change include the effects of changing normal stress. These problems were eventually overcome to varying degrees by several investigators (Teufel 1981, Raleigh & Marone 1986); however, these studies were carried out for different purposes and did not address variations in the friction rate parameter specifically.

The first detailed studies of the relationship between porosity changes and friction rate dependence were carried out by Morrow et al (1986), Marone & Scholz (1988, 1989), Morrow & Byerlee (1989), and Marone et al (1990). Morrow and coworkers documented a relationship between velocity-strengthening frictional behavior and pore volume in gouge layers. They emphasized the state of gouge consolidation and argued that friction velocity dependence derived from changes in the absolute value of porosity as a function of strain rate (Morrow & Byerlee 1989). On the other hand, Marone and coworkers focused on the rate of porosity change with shear strain and quantitatively evaluated the relationship between dilatancy rate and friction. They recognized that frictional

strength depends on the rate of change of porosity, rather than on its absolute value, and introduced the following relation based on the total work expended during shear per unit volume:

$$\tau = \tau_f + \sigma' d\phi/d\gamma, \tag{7}$$

where τ is the measured shear strength due to frictional strength τ_f and volumetric work against the effective normal stress σ' (Marone et al 1990). Equation 7 expresses the fact that the bulk shear strength for a deforming material is larger if the material is dilating during a given strain increment. Thus the measured frictional strength τ/σ' is expected to vary with the dilatancy rate [see works by Marone (1991), Scott et al (1994), and Beeler & Tullis (1997) for more extensive discussions].

Figure 9 shows data from Marone et al (1990) for a layer of quartz gouge sheared at constant normal stress of 150 MPa within rough surfaces. The data indicate strong velocity strengthening and significant velocity dependence of the dilatancy rate. Comparison of the dilatancy rate with that prior to a velocity

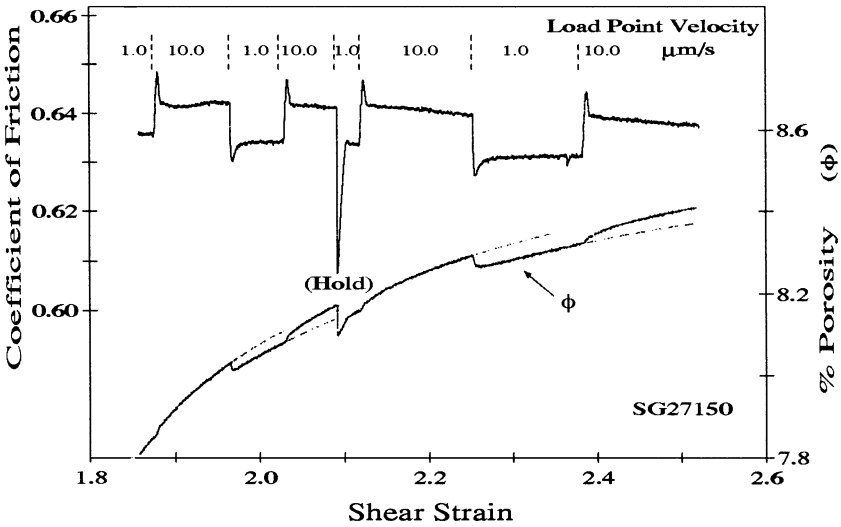

Figure 9 Friction and porosity data are shown versus average shear strain for a series of velocity stepping tests. The data show velocity strengthening frictional behavior and variations in the dilatancy rate as a function of load point velocity. *Dashed lines* indicate extrapolations of the porosity data prior to velocity steps. Note transient and short-term steady-state changes in dilatancy rate due to changes in loading point velocity. Data are for quartz gouge sheared within rough surfaces at a constant normal stress of 150 MPa and in the presence of water at room temperature. (Figure and data from Marone et al 1990.)

step indicates both a transient and a short-term steady-state effect of slip rate (Figure 9). The velocity-dependent changes in dilatancy rate occur over the same slip intervals as those of friction. By accounting for the measured velocity dependence of $d\phi/d\gamma$ (Equation 7), Marone et al (1990) were able to quantitatively explain the observation of velocity-strengthening friction in gouge. From Equation 7 recast in terms of friction, $\mu = \mu_f + d\phi/d\gamma$, the measured velocity dependence of friction $a - b = d\mu/dlnV$ is expected to include velocity dependence of the dilatancy rate $d(d\phi/d\gamma)/dlnV$. Marone et al (1990) found quantitative agreement between the steady-state effects when the velocity dependence of the μ_f term was included. In addition, their measurements of velocity-dependent dilatancy (Figure 10) showed the same systematic variations with gouge layer thickness and roughness as the friction measurements (Figure 7).

Based on these observations, the interpretation of the basic difference between friction of bare rock surfaces and granular fault gouge is simply that shear between rock surfaces does not involve significant dilation. This is

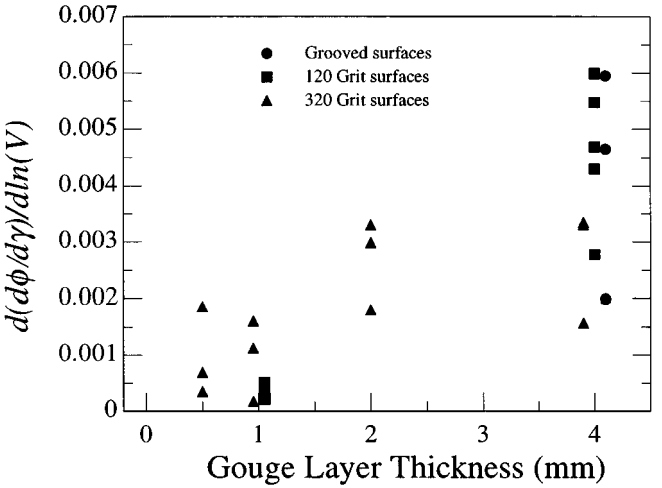

Figure 10 Systematic variations with layer thickness are shown for the variation in dilatancy rate with velocity, as measured from data such as shown in Figure 9. The ordinate represents the expected effect on the coefficient of friction due to volumetric work (Equation 7). Within the scatter, the data indicate quantitative agreement between observations of velocity strengthening and velocity dependence of the dilatancy rate when the effect of intrinsic velocity weakening as measured in bare-surface experiments is accounted for. The data are taken from the same tests shown in Figure 7. (Figure and data from Marone et al 1990.)

consistent with measurement (Marone et al 1990, Kilgore et al 1993, Wang & Scholz 1994, Beeler et al 1996). The same applies for shear within thin layers of gouge, since the data of Figure 10 indicate that velocity dependence of the dilatancy rate decreases for thinner layers. The fundamental implication of these data is that the granular nature of fault gouge, involving dilation during shear, produces velocity-strengthening frictional behavior (Marone et al 1990).

Beeler et al (1996), in a detailed study of granite gouge, also reported a relationship between friction velocity dependence and the dilatancy rate. Their experiments were performed in rotary shear, and they documented a clear correlation between steady-state friction velocity dependence and the rate of change of sample length with displacement $dL/d\delta$ (their Figure 6). As indicated in Figure 8, they observed a transition from velocity strengthening at low displacements to velocity weakening. At larger displacements, they found a transition back to velocity strengthening of approximately equal magnitude to that observed initially ($a - b \sim 0.002$). Their measurements of $dL/d\delta$ show exactly the same behavior as a function of slip: $dL/d\delta$ is large initially, it drops for displacements of about 30–100 mm, and then it increases to about the initial level for larger displacements. However, their values of $dL/d\delta$ during velocity strengthening are generally about 0.0005, whereas their corresponding measurements of $a - b$ range from 0.0005 to 0.002. Thus they do not always observe sufficiently large changes in the dilatancy rate to quantitatively explain velocity strengthening. The reason for the apparent discrepancy with the results of Marone et al (1990) is unclear. There are several differences between the experiments, including total displacement, normal stress, the presence of water, state of gouge consolidation, and the method used to measure changes in the dilatancy rate, and it is possible that one of these factors is the cause. However, the consistency and systematic nature of Beeler et al's (1996) observed relationship between friction velocity dependence and dilatancy rate suggest an underlying connection in the mechanism.

The Role of Shear Localization and Microstructures

A simple extension of the velocity-strengthening mechanism discussed would imply that the transition distance D_t observed for shear of gouge (Figure 8) represents the point at which the gouge layer no longer behaves as a (dilating) granular aggregate. From the detailed microstructural observations that have been carried out to date (e.g. Logan et al 1992, Beeler et al 1996), this indeed appears to be the case.

The observations of Logan et al (1992), who also summarized several earlier studies, show that shearing within gouge is pervasive up to about the

post-yield region (Figure 11), after which oblique R_1 Riedel shears begin to form. Figure 11 (after Logan et al 1992) shows a range of initial stress-strain behaviors to illustrate observed differences as a function of consolidation state and gouge materials. The onset of shear localization is associated with a significant change in dilatancy rate (Marone & Scholz 1989) and reduction in comminution rate of the bulk gouge layer (Sammis et al 1987). Logan et al (1992) show that with continued deformation in the post-yield region, Riedel shears become pervasive and link to B or Y boundary-parallel shears (Figure 11).

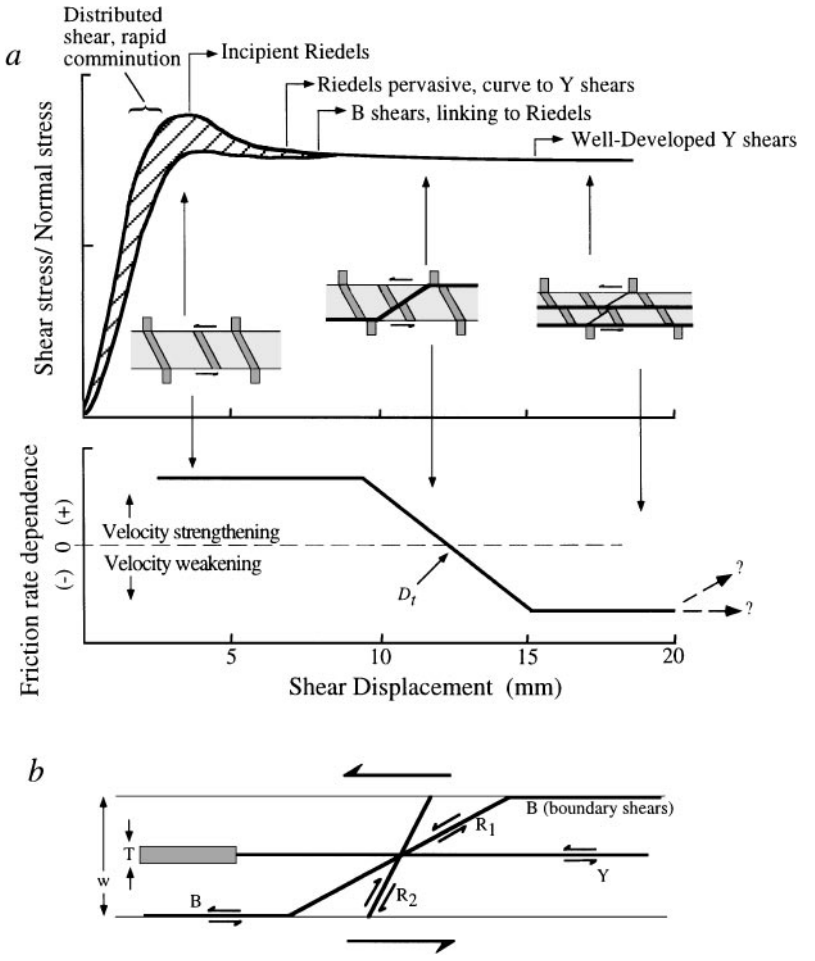

These shears generally initiate along one of the boundaries of the gouge layers (Beeler et al 1996), and for rough surfaces, there is a significant interval over which shear is accommodated by linkage between partial boundary shears (B shears of Figure 11) and R_1 shears (Marone et al 1990). Logan et al (1992) distinguished through-going boundary parallel shears as Y shears, and thus B shears are transient features. A stable frictional strength is reached at the point at which well-developed Y shears become prominent.

Also shown in Figure 11 is a sketch of friction rate dependence based on the data of Figure 8 and the microstructural observations of Logan et al (1992) and others. The curve is consistent with the most complete study to date (Beeler et al 1996), in which detailed friction data have been combined with microstructural observations of gouge. Beeler and coworkers found that velocity strengthening or velocity neutral behavior persists until a well-developed set of Y shears form. Pervasive deformation and slip localized along R_1 shears is associated with velocity strengthening (Marone et al 1990, Beeler et al 1996). Slip becomes concentrated on Y shears after 10–20 mm of displacement, and, as discussed above, this transition distance may be identified with D_t, which is expected to vary with factors such as surface roughness, gouge layer thickness, and initial particle-size distribution (e.g. Gu & Wong 1994). Figure 11 is drawn to show behavior only out to displacements of about 20 mm, and in this range, there is substantial agreement between the microstructural studies and friction behavior from a number of experimental testing geometries.

However, for larger displacements, which are attainable only in rotary shear, Beeler et al (1996) found a transition back to velocity strengthening. Their

←

Figure 11 Summary of the relationship between frictional shear strength, friction rate dependence, and the development of microstructures within fault gouge. (*a*) Sketches of gouge microstructures showing hypothetical markers across the gouge zone and bounding surfaces. Strain and offset of the markers illustrate the transition from pervasive deformation to localized shear. Zones of active shear are shown with *heavier lines* and indicate a transition from shear on oblique R_1 (Riedel) shears to boundary-parallel features. B shears represent partial Y shears along the gouge boundary. Y shears form at larger displacements and offset R_1 shears. Velocity strengthening is associated with pervasive strain and shear along R_1 features. D_t represents the transition displacement from velocity strengthening to weakening and is expected to vary with surface roughness, particle size, and, for rough surfaces, layer thickness. The onset of velocity weakening is associated with the development of Y shears, but in rotary shear experiments (Beeler et al 1996), these become unstable at larger displacements than the range shown here, and a transition occurs back toward velocity strengthening. (*b*) Definition of gouge microstructures following nomenclature of Logan et al (1992). T shows (at an extremely exaggerated scale) the width of localized slip along a Y shear band.

mechanical data from different tests show substantial variation; however, a trend toward increasing $a - b$ with displacement beyond about 50 mm is observed in each data set (figure B1 of Beeler et al 1996). Although the reason for this transition is as yet poorly understood, the microstructural observations are apparently consistent with those for smaller displacements (Figure 11). Beeler et al (1996) reported that for intermediate displacements of about 60 mm, deformation is concentrated in a narrow region of Y shears near one boundary of the gouge layer, with the rest of the layer essentially undeformed relative to the starting material. For much larger displacements, after the transition back toward velocity strengthening, they report that the region of intense shearing and comminution has widened significantly and contains a series of R_1 shears offset by Y shears. Because activation and slip along R_1 shears is associated with velocity strengthening (Figure 11), the data are consistent with the idea that velocity weakening only persists for localized slip along Y shears. Moreover, their observations of increased dilatancy for velocity strengthening are also consistent with the action of R_1 shears.

Although the results for the largest-displacement experiments are somewhat puzzling, the overall consistency of results from these and other experiments, and the systematic relationships between frictional behavior and microstructure, provide a substantial framework within which to tackle the problem of scaling results to natural faults. The data show clearly that a key element of the scaling problem is that of identifying microstructural features within active fault zones. Also, the connection must be made between the effects of surface roughness and particle size in laboratory experiments and mature fault zones.

Scaling of the Critical Slip Distance for Seismic Faulting

Notwithstanding the significance of the friction rate parameter and the problem of understanding its application to faulting, perhaps the most important scaling parameter in applying laboratory-derived friction laws in nature is the critical slip distance. As the parameter that sets the friction breakdown distance, D_c is the key factor in determining several fundamental aspects of seismic rupture, including the size of the rupture nucleation dimension, the spatial scale over which short-term precursory changes in physical properties may be expected, the magnitudes of pre- and postseismic slip, and the length scale over which dynamic stress is concentrated at the front of a propagating rupture (Dieterich 1986, Scholz 1988a, Lorenzetti & Tullis 1989, Shibazaki & Matsu'ura 1992, Marone & Kilgore 1993, Rice & Ben-Zion 1996). Moreover, unlike the situation for the friction rate parameter, for which there is rough agreement between laboratory values and field or modeling-based estimates, laboratory measurements of the critical slip distance are generally in the range of 10^{-6}–10^{-5} m; thus,

they are many orders of magnitude smaller than field-based estimates and those values required by dynamic rupture (Tse & Rice 1986, Power & Tullis 1992, Rice 1993, Beeler & Tullis 1996, Ben-Zion & Rice 1997). However, laboratory fault zones are much smaller than natural faults that are of interest, and thus the problem of scaling D_c must be addressed mechanistically and with models derived from laboratory-based interpretations of friction memory effects and state evolution.

Since the introduction of the rate and state friction laws, the standard interpretation of the critical slip distance has been that of the slip necessary to renew surface contacts (Dieterich 1979, 1981). (A similar interpretation can be made for slip-weakening constitutive models; Ohnaka & Yamashita 1989, Ohnaka 1996.) For shear between rock surfaces, this is an appealing model for several reasons. 1. It provides a clear connection between second-order variations in friction and models of base friction (the μ_o term in Equation 1), which derive from contact theory. 2. It offers a simple explanation for the relationship between observations of time-dependent friction and time-dependent contact indentation. 3. It is consistent with interpretations and direct measurements of friction in metals. 4. It makes simple predictions about the effects of surface roughness and particle size for gouge, which are supported by laboratory data (Dieterich 1981, Okubo & Dieterich 1984, Ohnaka & Kuwahara 1990). In addition, recent direct measurements of friction and contact area between plastics, which show the same type of rate- and state-dependent friction behavior as rock (Figure 6), show that changes in friction occur over essentially exactly the same distance as changes in contact area (Dieterich & Kilgore 1994).

Thus, one approach to the problem of scaling D_c is to simply account for the roughness of natural faults and compute the expected size of contact junctions, which should differ from D_c if at all by only a geometric factor. This approach was followed by Scholz (1988a), who by accounting for the fractal nature of fault surface roughness, found contact junction sizes of 10^{-3}–10^{-2} m for the depth range 6–20 km on mature faults, which is in good agreement with field-based estimates of D_c. However, this model ignores the presence of fault gouge and is thus incompatible with a number of other scaling models relating laboratory friction data to earthquake faulting and the seismic cycle (e.g. Sleep & Blanpied 1992, Miller 1996, Miller et al 1996, Scott 1996). To account for the effect of fault gouge, the mechanistic interpretation of D_c has to be reevaluated.

In the standard interpretation of D_c as applied to fault gouge, the particle size sets the contact junction dimension, and thus D_c should scale as such. Therefore, Dieterich's (1981) measurements showing that D_c scales with initial particle size of gouge are consistent with this model. However, Dieterich's data and those of others (Biegel et al 1989, Marone et al 1990) also show that D_c varies

with surface roughness. This variance would be explained by a relationship between contact junction size and surface roughness (Okubo & Dieterich 1984); however, the surfaces do not interact directly in these experiments. The gouge layer thickness (typically $\geq$1 mm) is significantly larger than the maximum surface topography (typically $<$50 μm). Thus, the observed scaling of D_c with surface roughness in experiments with gouge cannot be explained by the standard interpretation of D_c.

This led Marone & Kilgore (1993) to investigate the relationship between D_c and gouge layer thickness. They studied a range of initial particle sizes and gouge layer thicknesses and found that D_c varied systematically with particle size and shear strain (Figure 12). They found that the effect of particle size was small compared to that due to shear strain. For gouge composed of particles differing in size by more than a factor of 100, D_c changed by less than a factor of 2, whereas for each of the three initial particle sizes studied, D_c decreased by about a factor of 10 for a shear strain of 10 (Figure 12). Thus, Marone & Kilgore (1993) argued that the observed reduction in D_c was not a comminution effect. Instead, on the basis of microstructural observations such as those summarized above, they suggested that the reduction in D_c with shear strain was due to shear localization. Moreover, using high-resolution measurements of changes in layer thickness, they documented a direct correlation between D_c and the change in layer thickness, $\alpha = dw/dlogV$, upon an imposed velocity perturbation (Figure 12), where w is layer thickness (Figure 11). Similar observations have been reported by Wang & Scholz (1994) and Beeler et al (1996).

From their laboratory measurements and observations, Marone & Kilgore (1993) suggested a new interpretation of D_c for shear within fault gouge. In this model, D_c scales with the thickness of active shear:

$$D_c = \zeta T, \tag{8}$$

where ζ is a constant and T is the shear band thickness (shown at a greatly exaggerated scale in Figure 11). From their laboratory data, they inferred ζ of 10^{-2}. The model retains a relationship between D_c and particle size because shear bands encompass many particles, and hence shear consists of slip between a series of interparticle contacts. The model also predicts a surface roughness effect on D_c if shear is localized along or near the boundary.

This model suggests a different approach to the problem of scaling laboratory measurements of D_c to fault zones. That is, Equation 8 indicates that if the active shear zones can be identified in mature faults, the critical slip distance can be determined. Marone & Kilgore (1993) estimated $D_c = 1$ mm for an exhumed section of the San Andreas fault using the field data of Chester et al (1993), which shows $T = 10$ cm. As with the other scaling estimate noted above, this value is in reasonable agreement with field-based estimates. Thus, the problem

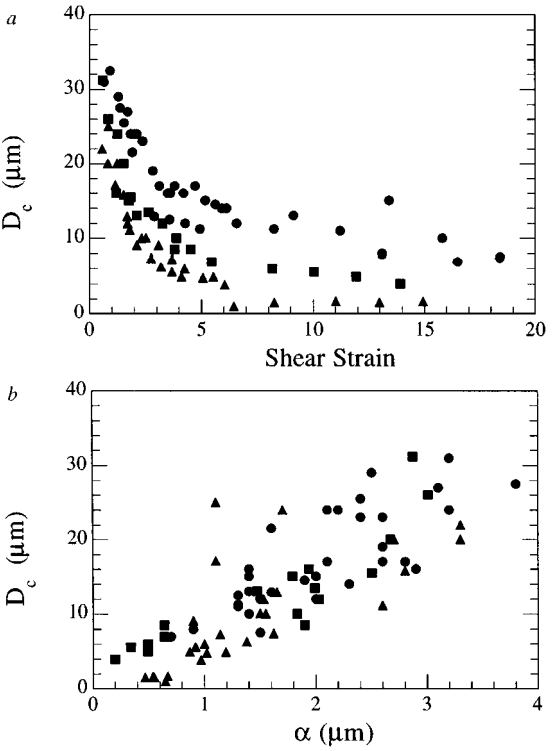

Figure 12 (*a*) Systematic variation of the critical slip distance as a function of initial particle size and shear strain for quartz gouge sheared within rough surfaces. Data from a number of experiments with different initial layer thicknesses are shown. *Coarse* (*circles*, 700 μm) and *fine* (*triangles*, 5 μm) indicate particles in a very narrow size range; *fractal* (*squares*, 20–700 μm) indicates a power-law size distribution over the range given. The systematic reduction in D_c with shear strain is interpreted as the result of shear localization. (*b*) Measurements of D_c are shown versus the instantaneous change in layer thickness for a velocity perturbation, $\alpha = dw/dlogV$, where w is layer thickness. α is interpreted as a proxy for shear band width T (see Figure 11), and thus the data indicate that D_c scales with shear band width (Equation 8). (Figure and data from Marone & Kilgore 1993.)

of scaling D_c is handled by a model that explains all of the available laboratory data.

Summary

Although we are still far from understanding the scaling problem in detail, several aspects of laboratory observations have been clarified by recent work. In particular, the role of dilatancy and fault gouge in producing velocity-strengthening frictional behavior and the observed differences in constitutive

parameters for rock-on-rock sliding versus shear within fault gouge are important. Unfortunately, with the exception of extreme cases (such as for shear within unconsolidated fault gouge or sediments, which from the foregoing discussion would be expected to exhibit velocity-strengthening frictional behavior, and slip within indurated or lithified materials, which would be expected to exhibit velocity weakening), the available data do not provide a clear answer to the problem of distinguishing the detailed conditions under which stable or unstable behavior is expected. As discussed in the next section, the best approach to this problem continues to be detailed analysis of seismic data and modeling of field observations. Finally, progress in understanding the role of shear localization and microstructures suggests that a mechanistic interpretation of friction is perhaps not far off. However, lack of detailed knowledge about fault zone characteristics, including material properties and microstructural conditions, continues to represent a significant barrier to developing realistic scaling models.

EARTHQUAKE AFTERSLIP AND THE RHEOLOGY OF MATURE FAULT ZONES

Since it was first documented following the 1966 Parkfield earthquake (Smith & Wyss 1968), afterslip has been observed for many earthquakes in a variety of settings. The best-documented cases tend to involve faults that are part of the San Andreas plate boundary system, but afterslip has also been documented for the M_s-7.5 1976 Guatemala earthquake (Bucknam et al 1978) and, recently, in large-scale interplate thrust settings (Heki et al 1997). Early work showed that the afterslip mechanism is distinct from seismic moment release associated with aftershocks (Scholz et al 1969), and thus workers recognized that afterslip could provide unique information on fault zone rheology (Nason & Weertman 1973, Crough & Burford 1977, Wesson 1988, Boatwright et al 1989, Marone et al 1991, Wennerberg & Sharp 1997). Initial investigations focused on creep events and empirical descriptions of afterslip using rheologies taken from plasticity. These purely empirical laws provide good fits to data. They are also of practical use for predicting total fault offsets following coseismic slip (Behr et al 1994) and for distinguishing between seismic and postseismic slip when incorporating paleoseismic data in studies of seismic hazards (Lienkaemper et al 1991, Jackson et al 1995, Bilham & Whitehead 1997).

However, as additional data sets became available, two things became clear. First, not all earthquakes produce appreciable afterslip, and even for dominantly strike-slip events on subvertical faults, where most afterslip events are observed, the correlation is inconsistent (e.g. Galehouse 1990, Sylvester 1993). Second, when afterslip does occur, there is a strong inverse correlation between

along-strike variations in coseismic slip and afterslip. These observations could be described by attributing differences in fault behavior to differences in quasi-plastic rheologies; however, in addition to being ad hoc, this does not provide explicit coupling between coseismic slip and afterslip. Moreover, rather than using a rheology based on plasticity to describe a brittle process, there is a distinct advantage in using a fault rheology that is capable of reproducing, and being tested by, laboratory experiments and other aspects of seismic faulting. The rate and state friction laws provide a natural candidate (Marone et al 1991). They contain both the slip and velocity-weakening characteristics necessary to generate earthquake-like instability and the viscous, velocity-strengthening response needed to reproduce transient strengthening and relaxation such as for afterslip. Here, I summarize such a model; I follow the discussion in Marone et al (1991), with particular focus on the comparison of faults with and without mature gouge zones and on the issue of using afterslip and other field data to evaluate the field application of laboratory-based friction laws. Also, incorporation of a new data set, from the 1992 Landers earthquake, provides an end-member test of the afterslip model.

Afterslip represents slip on a discrete fault or across a discrete fault zone, and it is generally measured by direct observation at the surface (e.g. Sharp et al 1982, 1989, Schulz 1984, Sylvester 1993) or inferred from geodetic measurements after correcting for elastic distortion in the crust (Crook et al 1982, Heki et al 1997). Although it is a postseismic phenomenon, afterslip is distinct from large-scale postseismic relaxation of crustal strain arising from viscoelastic interaction with the lower crust and uppermost asthenosphere (Rundle & Jackson 1977, Shen et al 1994, Pollitz 1997). The latter typically involves time scales of a year or more, and measurements are derived from wide-aperture geodetic arrays, for which the frequency of observations is often insufficient to unequivocally distinguish between coseismic and early postseismic deformation. Also, the deformation is generally inferred to be distributed and deep rather than concentrated on the fault that slipped seismically. In contrast, afterslip involves shorter time scales, with typical data showing half of the first year's afterslip within the first fortnight (Figure 13). A common feature of afterslip observations is a rapid initial rate of slip and a logarithmic decay in slip rate back toward the long-term interseismic rate (Figure 13). Creep events, of which afterslip is comprised, also show this form (Schulz et al 1982, Bilham & Whitehead 1997). Afterslip magnitude varies greatly, but in some cases, the ratio of afterslip to average coseismic fault slip approaches or exceeds 1 (e.g. Heki et al 1997).

Figure 13 shows afterslip measurements from four well-studied strike-slip earthquakes: the M_L-5.8 1966 Parkfield, M_s-7.5 1976 Guatemala, M_s-6.6 1987 Superstition Hills, and M_w-7.3 1992 Landers earthquakes. Afterslip is often

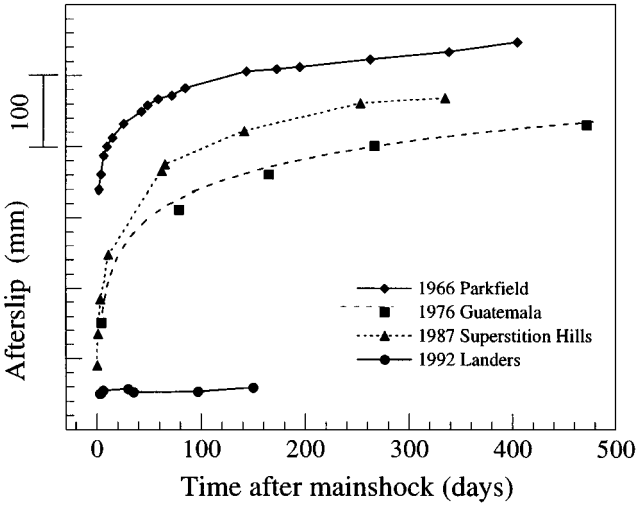

Figure 13 Afterslip measurements from four well-studied earthquakes. Three of the events indicate significant afterslip, with the ratio of the first year's afterslip to average coseismic slip approaching 1, whereas the 1992 Landers event shows negligible afterslip. The afterslip data and the lack of afterslip for the Landers event are explained by a model in which afterslip is driven by a coseismic slip deficit and laboratory-derived friction laws. Data are from Smith & Wyss (1968) (Parkfield), Bucknam et al (1978) (Guatemala), Williams & Magistrale (1989) (Superstition Hills), and Sylvester (1993) (Landers).

measured using temporary fiducial marks installed a few hours or days after the mainshock, and thus they generally represent only relative offset, which is the way they are shown in Figure 13. Three of the events show "typical" afterslip curves with magnitudes from 15 to 35 cm and durations that exceed one year (data from Smith & Wyss 1968, Bucknam et al 1978, Williams & Magistrale 1989). The fourth, the Landers event, shows negligible afterslip, although detailed measurements were carried out at several locations along the fault (Sylvester 1993). An obvious question is why does the Landers event not show afterslip?

Evidence for Coupling Between Coseismic Slip and Afterslip

Beginning with the early work by Smith & Wyss (1968), afterslip was recognized to exhibit an inverse relationship with coseismic slip. These authors also noted a correlation between afterslip and the presence of sediments, which was confirmed as subsequent data sets became available (Bucknam et al 1978, Harsh 1982, Sharp et al 1982, 1989, Schulz 1984, Williams & Magistrale 1989,

Sylvester 1993). The coupling between coseismic slip and afterslip and the connection with unconsolidated material occurs at two scales. By its nature, the first applies only to earthquakes for which afterslip is observed. In such cases, along-strike irregularities of coseismic surface slip correlate inversely with afterslip, which has the effect of smoothing the net slip distribution over time. The correlation between afterslip and coseismic slip holds for points within the central portion of the rupture trace, such as step-overs and geometric irregularities, and for the rupture ends, where afterslip tends to increase as coseismic slip tapers off (e.g. Sharp et al 1989, Sylvester 1993, Behr et al 1994). However, many factors influence afterslip, and thus the generality of these statements is limited. For example, the lack of detection of afterslip could be associated with very large, as indicated by the preceding discussion, or very small coseismic slip, inasmuch as coseismic slip is a basic driving force for afterslip and postseismic deformation.

The connection between afterslip and coseismic slip is also apparent at a larger scale, where it involves strong depth variation of coseismic slip. The available data indicate that earthquakes with significant afterslip within the limits of the initial rupture extent tend to be those that involve buried coseismic slip. Examples include the 1966 Parkfield, the 1979 Imperial Valley, the 1984 Morgan Hill, and the 1987 Superstition Hills earthquakes. For these events, surface slip deficits are indicated by inversion of seismic strong motion records and/or geodetic inversions or by comparison of measured surface slip with that inferred from seismic moment. Figure 14 shows an example from the 1987 Superstition Hills earthquake (Wald et al 1990). Rupture nucleated at a depth of about 9 km and propagated nearly 20 km along strike but only 5 km updip. Coseismic slip decreased rapidly at 4–5 km, producing elongated oval-shaped slip contours (Figure 14). This shape is characteristic of the coseismic slip contours of earthquakes that show appreciable afterslip (Hartzell & Heaton 1983, Archuleta 1984, Beroza & Spudich 1988, Segall & Du 1993).

Figure 14 also shows the coseismic slip distribution for the 1992 Landers earthquake (Wald & Heaton 1994). Although this event nucleated at a depth similar to that for the Superstition Hills event, rupture extended coseismically to the surface and the slip contours show no shallow slip deficit. Taken together with the afterslip data (Figure 13), this implies that the large-scale inverse correlation between coseismic slip and afterslip extends to the extreme case. That is, afterslip requires that there be a coseismic slip deficit. However, a fairly straightforward extension of this statement, that afterslip is driven by the coseismic slip deficit and occurs primarily in that region, was not recognized until quite recently (Crook et al 1982, Marone et al 1991). Crook et al (1982) made geodetic observations and afterslip measurements following the 1979 Imperial Valley earthquake and showed that afterslip there was essentially a shallow

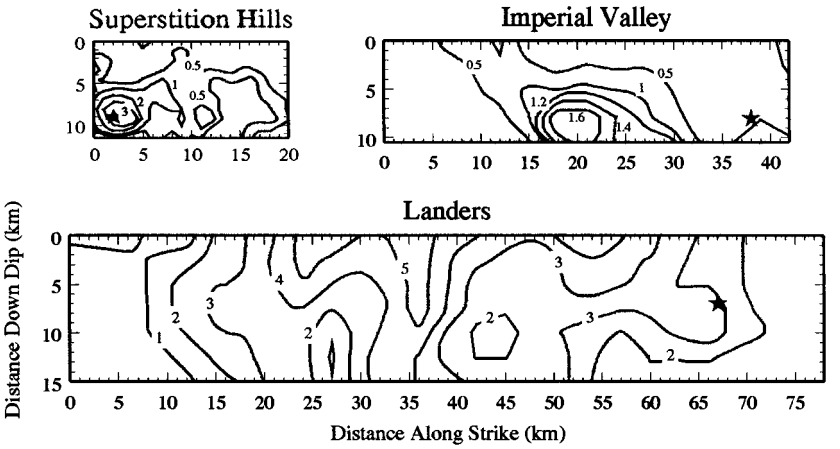

Figure 14 Contours of coseismic slip in meters as a function of depth and distance along strike for three well-studied California earthquakes. Data are from inversions of seismic strong motion records by Wald et al (1990) (1987 Superstition Hills), Hartzell & Heaton (1983) (1979 Imperial Valley), and Wald & Heaton (1994) (1992 Landers). *Stars* indicate earthquake hypocenters. The data for Superstition Hills and Imperial Valley indicate buried slip, with significant reduction in coseismic slip above about 5 km. These events show significant afterslip. In contrast, for the Landers event, strong coseismic slip extends directly to the surface, and this event exhibited negligible afterslip. (Data and figure provided by D Wald.)

process, occurring in that case within the upper 4–5 km. If afterslip is carefully distinguished from large-scale postseismic deformation, as noted above, then this finding is not inconsistent with previous observations or interpretations. However, previous work on afterslip had focused on either the detailed structure of creep events or deep-seated postseismic deformation and its implications for asthenosphere viscosity. Afterslip had not been connected with the cause of buried coseismic slip nor with field data such as crustal structure and the depth distribution of seismicity.

A Synoptic Model for Mature Fault Zones: The Role of Fault Gouge

If we accept a connection between afterslip and the existence of a coseismic slip deficit, located in the shallow portion of California strike-slip faults and presumably deeper for the subduction zone observations of Heki et al (1997), what remains is to connect these observations in a mechanical model that accounts for seismic data and other field observations. Figure 15 shows such a synoptic model based on that introduced by Marone et al (1991). The primary feature of the model is a wide mature zone of unconsolidated fault gouge

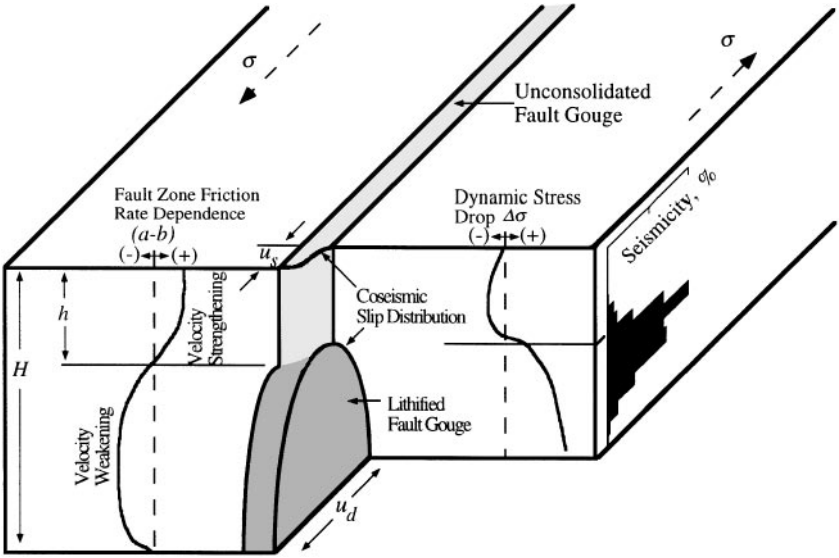

Figure 15 Synoptic model for earthquake afterslip illustrating the relationship between frictional properties and seismic behavior of a mature crustal fault zone. The *shaded region* shows unconsolidated fault gouge extending from the surface to depth h and lithified gouge below extending to the base of the seismogenic zone at depth H. The coseismic slip distribution for a hypothetical earthquake with buried slip is shown. The average surface slip is u_s, whereas slip at depth is u_d. The histogram at the far right shows the depth-frequency distribution of well-located seismicity along the Imperial fault for the period 1977–1983 (Doser & Kanamori 1986) and illustrates the relationship between friction rate dependence and seismic stability. The *curve* showing dynamic stress drop as a function of depth is drawn to be consistent with the laboratory and seismic data. The model shows that velocity-strengthening frictional behavior within the upper region of mature faults is expected to result in a stability transition, resulting in a lack of seismicity above depth h and arrest of coseismic slip within this region. This model is used to describe earthquake afterslip, which is driven by the coseismic slip deficit and rate/state frictional rheology. (Modified from Marone et al 1991.)

extending to depth h within an elastic plate of thickness H. In the context of this model, the existence of a significant gouge zone is the defining feature of a mature fault zone. As argued by Marone & Scholz (1988) and discussed below, faults that do not have an appreciable gouge zone (immature faults) behave in a fundamentally different way.

The model illustrates the coseismic slip distribution immediately following a moderate-sized strike-slip earthquake. A slip deficit is shown above depth h, which is consistent with the data shown in Figure 14. Also shown is the friction rate dependence $(a - b)$ within the fault zone as a function of depth

(Figure 15). The curve is drawn to show two stability transitions: an upper one at depth h, associated with the transition from unconsolidated gouge to lithified and indurated gouge, and a second transition at depth H, associated with increasing temperature. The form of the velocity-weakening curve and the transition back to positive $a - b$ at depth is based on work showing variations in friction behavior (Stesky 1978) and constitutive parameters (Blanpied et al 1991, 1995, 1997) with increasing temperature, which are presumed to result from a transition to plastic deformation, as summarized by Scholz (1988b, 1990). The upper stability transition is based on laboratory measurements showing that unconsolidated gouge exhibits velocity strengthening (Marone et al 1990). As discussed above, those data show that dilation is the fundamental cause of velocity strengthening within granular aggregates (Marone et al 1990, Beeler et al 1996), notwithstanding the possible role of clays and serpentine (Reinen et al 1994, Moore et al 1996). Hence, although it is unlikely that fault zones are comprised of completely unconsolidated material, they need only dilate and deform as an aggregate, rather than an intact rock, in order to exhibit velocity-strengthening friction. Below depth h, the fault zone is shown to be consolidated and velocity weakening in character (Figure 15).

The details of the upper stability transition are poorly understood; however, this depth is presumed to represent a dynamic balance between physicochemical processes that cause lithification and consolidation, on the one hand, and the disaggregating effects of abrasive wear, including microfracturing and brecciation within the fault zone and surrounding country rock. The latter effects are driven primarily by slip, and the former by time and chemical processes; thus active slip is a fundamental requirement for the existence of a mature fault zone. Faults with low slip rates and long seismic recurrence intervals would not be expected to exhibit mature characteristics.

Laboratory data suggest the general form of the friction rate curve, which can be used to make specific predictions regarding field applications; however, owing to uncertainties in scaling parameters and incomplete knowledge of fault materials, they do not provide detailed, independent constraints on the depth of the stability transitions. These need to be assessed from field data and modeling studies. One prediction of the friction data, coupled with stability analyses (Rice & Ruina 1983), is that earthquakes should not nucleate within the upper region of mature fault zones (Marone & Scholz 1988). Thus, the depth of the upper stability transition can be determined from seismic data.

On *the right-hand side* of Figure 15, I show high-resolution relocated seismicity data (Doser & Kanamori 1986) for the Imperial fault. Several other data sets are given by Marone & Scholz (1988). They show that active faults with mature gouge zones indicate a clear upper bound on seismicity, with $>90\%$ of the seismicity occurring below 3–5 km (Figure 15). Also shown is a sketch of

the dynamic stress drop that would be predicted for an earthquake nucleating at depth and rupturing a fault zone with the frictional properties given. The curve shows positive stress drop (dynamic frictional strength is lower than the initial stress level) in the lower region and a transition to negative stress drop above depth h. The region of negative stress drop indicates that the shallow portion of mature faults will act as strong barriers to seismic rupture. This in turn implies that the depth of the upper stability transition can be independently assessed from modeling studies of dynamic rupture. In the case of the 1979 Imperial Valley earthquake, Quin (1990) carried out such modeling and found negative stress drop in the region above about 5 km. Thus the laboratory data and field observations indicate that the upper region of mature fault zones exhibit velocity-strengthening friction. As a consequence, such faults should exhibit a coseismic slip deficit in this region.

The region of negative stress drop and the associated coseismic slip deficit provide the connection to a model for afterslip (Marone et al 1991). Basic features of the model are that fault gouge arrests coseismic slip in the shallow portion of mature faults and that afterslip is driven by relaxation of the resulting stress concentration. Both the coseismic slip deficit and afterslip characteristics can be described with a single model and rheology, given by a rate and state friction law. Marone et al (1991) used the Ruina law in their modeling and considered only single-degree-of-freedom elastic coupling between the fault and its surroundings, whereas recent work by Wennerberg & Sharp (1997) indicates that the Dieterich law is more appropriate in some cases. Interaction between the coseismically slipping region at depth and the upper region is accounted for with depth-averaged slip and stiffness. The model yields coseismic and postseismic surface slip as a function of the friction parameters, elastic properties, and the earthquake rise time (slip duration at depth).

Figure 16*a* shows some basic features of the model. The *curves* are calculated for a rise time of 1 s and $a - b$ of 0.005 within the velocity-strengthening region. They show surface fault slip at the end of the coseismic period and after one year, normalized by the coseismic slip at depth. As expected, coseismic surface slip diminishes with increasing h, since the energy required to propagate rupture through the velocity-strengthening region scales with h. Net surface slip after one year also decreases with h, since the relaxation time for afterslip increases with h (Figure 16*a*). Coseismic surface slip decreases more rapidly than afterslip, and thus the ratio of the two increases with increasing h. For h of about 1.75 km, the ratio of afterslip to coseismic surface slip is 1. Buried slip is implied for $h > 2.2$, and for values of $\sim$2.5 km, the first year's afterslip is about equal in magnitude to the average slip at depth. These parameters also scale with earthquake rise time (coseismic surface slip increases with rise time) and the degree of velocity strengthening within the fault gouge, which reduces

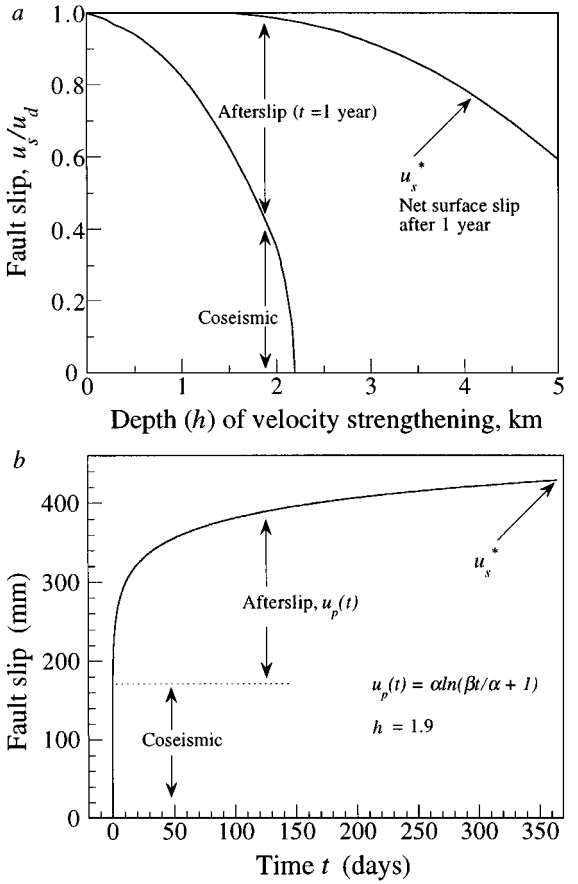

Figure 16 Coseismic slip and afterslip relations for the model illustrated in Figure 15. (*a*) *Lower curve* shows the ratio of coseismic slip at the surface to coseismic slip at depth, and *upper curve* shows the ratio of afterslip at the surface after 1 year to coseismic slip at depth. Each are shown versus the depth of the velocity-strengthening region h, according to the model of Marone et al (1991). Mature faults would correspond to large h. The *curves* indicate that for small values of h, significant coseismic slip extends to the surface and afterslip is negligible, whereas for larger values of h (see Figure 15), the opposite is true. (*b*) The complete temporal history of fault slip is shown for the afterslip model, including coseismic slip and afterslip within one year. The model is shown for a velocity-strengthening region of depth $h = 1.9$ km, and afterslip is calculated according to the relation given. (Data and model from Marone et al 1991.)

coseismic slip for a given set of conditions. Thus for large events and small values of h, all slip may be coseismic, whereas afterslip would occur for a more moderate-sized event.

Figure 16 also shows a time series of coseismic slip and afterslip, calculated using an analytic approximation to the full rate and state friction afterslip model (Scholz 1990, Marone et al 1991). In this relation, $\alpha = A-B/k$, where the upper case letters indicate shear stress equivalents of the friction parameters a and b, k is stiffness, and β is the depth-averaged coseismic slip velocity within the velocity-strengthening region. This relation reproduces the basic features of afterslip data, although it does not fit some aspects of the data as well as empirical laws with more free parameters (Marone et al 1991, Behr et al 1994).

Finally, because of the relation between the transition depth and effective stiffness, afterslip data can be inverted to yield estimates of the transition depth h. Marone et al (1991) inverted afterslip data from the 1966 Parkfield event and the 1987 Superstition Hills event, using laboratory friction values as a constraint, and found values for the depth of the velocity-strengthening region of 3–5 km, in good agreement with the independent estimates from seismic data and dynamic modeling. Wennerberg & Sharp (1997) used the same basic model but relaxed the assumption of steady-state friction behavior and carried out a detailed study of afterslip using data from the 1987 Superstition Hills earthquake. They also found good fits to the data. Their analysis showed that the Dieterich law provides a better fit to afterslip data than the Ruina law and that certain aspects of the data indicate two-state variable behavior.

SUMMARY COMMENTS

Despite the apparent success of our synoptic model in describing afterslip and providing explanations for its connection to a variety of seismic data, a major difficulty in testing the model is the prediction that afterslip will not occur in many cases. Afterslip is not expected on immature faults or on mature faults for which the coseismic rise time is too large or too small. If we take rise time as roughly equivalent to magnitude, the absence of afterslip for small events is not surprising. However, large events present a problem for testing the model, since the absence of afterslip could arise from the lack of a mature fault zone or from rupture propagation through the velocity-strengthening region without leaving a coseismic slip deficit.

The 1992 Landers event provides a good example for discussion. The rupture propagated unilaterally, and thus the rise time at a given location along strike was limited. However, the static stress drop was large, with up to 6 m of slip occurring on a 70-km-long fault. Strong motion inversions and geodetic observations show clearly that a shallow coseismic slip deficit did not exist.

Thus, in this limited sense, our model is correct in predicting no afterslip within the main rupture trace. However, is this due to the lack of a mature gouge zone, as could be argued based on the inferred long seismic recurrence interval, or to a particularly energetic rupture? If the fault zones involved in the Landers rupture had contained significant gouge, then perhaps the rupture would not have extended into the shallow region; however, this presumes many things about the nature of dynamic rupture propagation and the initial stress conditions that are very poorly understood.

As a closing comment, I note the rather obvious connection between the synoptic afterslip model described here involving mature fault zones and the recent observations and inferences for earthquake nucleation and slow and silent faulting on the San Andreas fault and elsewhere (Behr et al 1990, Beroza & Jordan 1990, Iio 1992, Ihmlé et al 1993, Kanamori & Kikuchi 1993, Gladwin et al 1994, Ihmlé & Jordan 1994, Ellsworth & Beroza 1995, Kawasaki et al 1995, Beroza & Ellsworth 1996, Ihmlé 1996, Linde et al 1996, McGuire et al 1996, DeMets 1997, Heki et al 1997). As discussed originally by Rice & Gu (1983), rate and state friction laws predict a spectrum of behaviors that range from aseismic creep, to transiently accelerating slip that does not reach instability, to slow precursive slip prior to fully dynamic instability. The latter two behaviors require somewhat specialized rheologic properties, such as approximately velocity-neutral friction behavior, a change in $a - b$ with velocity, or unusually large values of D_c; however, such behaviors have been observed in the laboratory (e.g. Reinen et al 1991, 1992, 1994, Ma & Toshihiko 1995, Blanpied et al 1997) or can be inferred from existing laboratory-based models of scaling (Marone & Kilgore 1993, Gu & Wong 1994). What remains is to devise specific laboratory tests of the field observations and/or to construct theoretical models that could be used to model infraseismic observations and place constraints on the range of permissible constitutive parameters.

ACKNOWLEDGMENTS

A number of people have contributed to my understanding of this topic. In particular I thank Jim Rice, Chris Scholz, Nick Beeler, Mike Blanpied, and Terry Tullis for patient discussions at different times that helped sharpen my understanding of various points. I have also benefited greatly from discussions and explanations by John Vidale and Tom Jordan on the interpretation and implications of seismic data. In producing this manuscript, I received help at key times from Steve Karner and Maureen Raymo, for which I am grateful. I thank Karen Mair, Steve Karner, and Nick Beeler for comments on the manuscript, which helped clarify several issues. I would also like to thank Dave Wald, Jim Dieterich, and Brian Kilgore for providing figures from their work and for doing so with extreme rapidity. This work was supported by National Science

Foundation grants EAR-9316082 and EAR-9627895 and by the Kerr-McGee foundation through a career development chair at the Massachusetts Institute of Technology.

Literature Cited

Abercrombie R, Leary P. 1993. Source parameters of small earthquakes recorded at 2.5 km depth, Cajon Pass, Southern California: implications for earthquake scaling. *Geophys. Res. Lett.* 20:1511–14

Andrews DJ, Ben-Zion Y. 1997. Wrinkle-like slip pulse on a fault between different materials. *J. Geophys. Res.* 102:553–71

Andrews J. 1976. Rupture propagation with finite stress in antiplane strain. *J. Geophys. Res.* 81:3575–82

Archuleta RJ. 1984. A faulting model for the 1979 Imperial Valley earthquake. *J. Geophys. Res.* 89:4559–85

Baumberger T, Heslot F, Perrin B. 1994. Crossover from creep to inertial motion in friction dynamics. *Nature* 367:544–46

Beeler NM, Tullis TE. 1996. Self-healing slip pulses in dynamic rupture models due to velocity dependent strength. *Bull. Seismol. Soc. Am.* 86:1130–48

Beeler NM, Tullis TE. 1997. The roles of time and displacement in velocity dependent volumetric strain of fault zones. *J. Geophys. Res.* 102:22595–609

Beeler NM, Tullis TE, Weeks JD. 1994. The roles of time and displacement in the evolution effect in rock friction. *Geophys. Res. Lett.* 21:1987–90

Beeler NM, Tullis TE, Weeks JD. 1996. Frictional behavior of large displacement experimental faults. *J. Geophys. Res.* 101:8697–715

Behr J, Bilham R, Bodin P, Burford RO, Burgmann R. 1990. Aseismic slip on the San Andreas fault south of Loma Prieta. *Geophys. Res. Lett.* 17:1445–48

Behr J, Bilham R, Bodin P, Gross S. 1994. Eureka peak fault afterslip following the 28 June 1992 Landers earthquake. *Bull. Seismol. Soc. Am.* 84:826–34

Ben-Zion Y. 1996. Stress, slip, and earthquakes in models of complex single-fault systems incorporating brittle and creep deformations. *J. Geophys. Res.* 101:5677–706

Ben-Zion Y, Rice JR. 1995. Slip patterns and earthquake populations along different classes of faults in elastic solids. *J. Geophys. Res.* 100:12959–83

Ben-Zion Y, Rice JR. 1997. Dynamic simulations of slip on a smooth fault in an elastic solid. *J. Geophys. Res.* 102:17771–84

Beroza GC, Ellsworth WL. 1996. Properties of the seismic nucleation phase. *Tectonophysics* 261:209–27

Beroza GC, Jordan TH. 1990. Searching for slow and silent earthquakes using free oscillations. *J. Geophys. Res.* 95:2485–510

Beroza GC, Spudich P. 1988. Linearized inversion for fault rupture behavior: application to the 1984 Morgan Hill, California, earthquake. *J. Geophys. Res.* 93:6275–96

Beroza GC, Zoback MD. 1993. Mechanism diversity of the Loma Prieta aftershocks and the mechanics of mainshock-aftershock interaction. *Science* 259:210–13

Biegel RL, Sammis CG, Dieterich JH. 1989. The frictional properties of a simulated gouge with a fractal particle distribution. *J. Struct. Geol.* 11:827–46

Biegel RL, Wang W, Scholz CH, Boitnott GN, Yoshioka N. 1992. Micromechanics of rock friction, 1. Effects of surface roughness on initial friction and slip hardening in westerly granite. *J. Geophys. Res.* 97:8951–64

Bilham R, Whitehead S. 1997. Subsurface creep on the Hayward fault, Fremont, California. *Geophys. Res. Lett.* 24:1307–10

Blanpied ML, Lockner DA, Byerlee JD. 1991. Fault stability inferred from granite sliding experiments at hydrothermal conditions. *Geophys. Res. Let.* 18:609–12

Blanpied ML, Lockner DA, Byerlee JD. 1992. An earthquake mechanism based on rapid sealing of faults. *Nature* 358:574–76

Blanpied ML, Lockner DA, Byerlee JD. 1995. Frictional slip of granite at hydrothermal conditions. *J. Geophys. Res.* 100:13045–64

Blanpied ML, Marone C, Lockner DA, Byerlee JD, King DP. 1997. Quantitative measure of the variation in fault rheology due to fluid-rock interactions. *J. Geophys. Res.* In press

Blanpied ML, Tullis TE. 1986. The stability and behavior of a frictional system with a two state variable constitutive law. *Pure Appl. Geophys.* 124:415–30

Blanpied ML, Tullis TE, Weeks JD. 1987. Fric-

tional behavior of granite at low and high sliding velocity. *Geophys. Res. Lett.* 14:554–57
Blanpied ML, Tullis TE, Weeks JD. 1998. Effects of slip, slip rate, and shear heating on the friction of granite. *J. Geophys. Res.* 103:489–512
Boatwright J, Budding KE, Sharp RV. 1989. Inverting measurements of surface slip on the Superstition Hills fault zone. *Bull. Seismol. Soc. Am.* 79:411–23
Boatwright J, Cocco M. 1996. Frictional constraints on crustal faulting. *J. Geophys. Res.* 101:13895–909
Boitnott GN, Biegel RL, Scholz CH, Yosioka N, Wang W. 1992. Micromechanics of rock friction, 2: quantitative modeling of initial friction with contact theory. *J. Geophys. Res.* 97:8965–78
Brace WF, Byerlee JD. 1966. Stick-slip as a mechanism for earthquakes. *Science* 153: 990–92
Brace WF, Byerlee JD. 1970. California earthquakes: Why only shallow focus? *Science* 168:1573–75
Bucknam R, Plafker CG, Sharp RV. 1978. Fault movement (afterslip) following the Guatemala earthquake of February 4, 1976. *Geology* 6:170–73
Byerlee JD. 1967. Frictional characteristics of granite under high confining pressure. *J. Geophys. Res.* 72:3639–48
Byerlee JD. 1978. Friction of rocks. *Pure Appl. Geophys.* 116:615–26
Byerlee JD. 1990. Friction, overpressure and fault normal compression. *Geophys. Res. Lett.* 17:2109–12
Byerlee JD, Summers R. 1976. A note on the effect of fault gouge thickness on fault stability. *Int. J. Rock Mech. Mining Sci. Geomech. Abstr.* 13:35–36
Cao T, Aki K. 1986. Effect of slip rate on stress drop. *Pure Appl. Geophys.* 124:515–29
Carlson JM, Langer JS. 1989. Mechanical model of an earthquake fault. *Phys. Rev. A* 40:6470–84
Carlson JM, Langer JS, Shaw BE, Tang C. 1991. Intrinsic properties of a Burridge-Knopoff model of an earthquake fault. *Phys. Rev. A* 44:884–97
Chester FM. 1994. Effects of temperature on friction: constitutive equations and experiments with quartz gouge. *J. Geophys. Res.* 99:7247–61
Chester FM. 1995. A rheologic model for wet crust applied to strike slip faults. *J. Geophys. Res.* 100:13033–45
Chester FM, Evans JP, Biegel RL. 1993. Internal structure and weakening mechanisms of the San Andreas fault. *J. Geophys. Res.* 98:771–86
Chester FM, Higgs NG. 1992. Multimechanism friction constitutive model for ultrafine quartz gouge at hypocentral conditions. *J. Geophys. Res.* 97:1857–70
Chester FM, Logan JM. 1987. Composite planar fabric of gouge from the Punchbowl fault, California. *J. Struct. Geol.* 9:621–34
Cochard A, Madariaga R. 1994. Dynamic faulting under rate-dependent friction. *Pure Appl. Geophys.* 142:419–46
Cochard A, Madariaga R. 1996. Complexity of seismicity due to highly rate-dependent friction. *J. Geophys. Res.* 101:25321–36
Cook NGW. 1981. Stiff testing machines, stick slip sliding, and the stability of rock deformation. In *Mechanical Behavior of Crustal Rocks*, ed. NL Carter, M Friedman, JM Logan, DW Sterns, Am. Geophys. *Union Monogr.*, 24:93–103. Washington, DC: Am. Geophys. Union
Crook CN, Mason RG, Wood PR. 1982. Geodetic measurements of horizontal deformation on the Imperial fault. In *The Imperial Valley Earthquake of October 15, 1979, US Geol. Surv. Prof. Pap.* 1254:183–91
Crough ST, Burford RO. 1977. Empirical law for fault-creep events. *Tectonophysics* 42:53–59
Das S, Boatwright J, Scholz CH, ed. 1986. *Earthquake Source Mechanics, Am. Geophys. Union Monogr.* Washington, DC: Am. Geophys. Union
DeMets C. 1997. Afterslip no longer an afterthought. *Nature* 386:549
Dieterich JH. 1972. Time-dependent friction in rocks. *J. Geophys. Res.* 77:3690–97
Dieterich JH. 1978. Time-dependent friction and the mechanics of stick-slip. *Pure Appl. Geophys.* 116:790–805
Dieterich JH. 1979. Modeling of rock friction: 1. Experimental results and constitutive equations. *J. Geophys. Res.* 84:2161–68
Dieterich JH. 1981. Constitutive properties of faults with simulated gouge. In *Mechanical Behavior of Crustal Rocks*, ed. NL Carter, M Friedman, JM Logan, DW Sterns, *Am. Geophys. Union Monogr.*, 24:103–20. Washington, DC: Am. Geophys. Union
Dieterich JH. 1986. A model for the nucleation of earthquake slip. See Das et al 1986, 37:37–47
Dieterich JH. 1992. Earthquake nucleation on faults with rate and state-dependent friction. *Tectonophysics* 211:149–78
Dieterich JH. 1994. A constitutive law for rate of earthquake production and its application to earthquake clustering. *J. Geophys. Res.* 99:2601–18
Dieterich JH, Conrad G. 1984. Effect of humidity on time and velocity-dependent friction in rocks. *J. Geophys. Res.* 89:4196–202
Dieterich JH, Kilgore B. 1994. Direct observa-

tion of frictional contacts: new insights for state-dependent properties. *Pure Appl. Geophys.* 143:283–302
Dieterich JH, Kilgore B. 1996a. Implications of fault constitutive properties for earthquake prediction. *Proc. Natl. Acad. Sci. USA* 93:3787–94
Dieterich JH, Kilgore B. 1996b. Imaging surface contacts; power law contact distributions and contact stresses in quartz, calcite, glass, and acrylic plastic. *Tectonophysics* 256:219–39
Dieterich JH, Linker MF. 1992. Fault stability under conditions of variable normal stress. *Geophys. Res. Lett.* 19:1691–94
Doser DI, Kanamori H. 1986. Depth of seismicity in the Imperial Valley region 1977–1983 and its relationship to heat flow, crustal structure, and the October 15, 1979, earthquake. *J. Geophys. Res.* 91:675–88
Edmond JM, Paterson MS. 1972. Volume changes during the deformation of rocks at high pressures. *Int. J. Rock Mech. Mining Sci. Geomech. Abstr.* 9:161–82
Ellsworth WL, Beroza GC. 1995. Seismic evidence for an earthquake nucleation phase. *Science* 268:851–55
Engelder JT, Logan JM, Handin J. 1975. The sliding characteristics of sandstone on quartz fault-gouge. *Pure Appl. Geophys.* 113:69–86
Engelder JT, Scholz CH. 1976. The role of asperity indentation and ploughing in rock friction II. *Int. J. Rock Mech. Mining Sci. Geomech. Abstr.* 13:155–63
Fredrich JT, Evans B. 1992. Strength recovery along simulated faults by solution transfer processes. *Proc. 33rd US Natl. Rock Mech. Symp.*, ed. W Wawersik, pp. 121–30. Rotterdam: Balkema
Galehouse JS. 1990. Effect of the Loma Prieta earthquake on surface slip along the Calaveras fault in the Hollister area. *Geophys. Res. Lett.* 17:1219–22
Gladwin MT, Gwyther RL, Hart RHG, Breckenridge KS. 1994. Measurements of the strain field associated with episodic creep events on the San Andreas fault at San Juan Bautista, California. *J. Geophys. Res.* 99:4559–65
Gross SJ, Kisslinger C. 1997. Estimating tectonic stress rate and state with Landers aftershocks. *J. Geophys. Res.* 102:7603–12
Gu JC, Rice JR, Ruina AL, Tse ST. 1984. Slip motion and stability of a single degree of freedom elastic system with rate and state dependent friction. *J. Mech. Phys. Solids* 32:167–96
Gu Y, Wong Tf. 1994. Development of shear localization in simulated quartz gouge: effect of cumulative slip and gouge particle size. *Pure Appl. Geophys.* 143:387–24
Harsh PW. 1982. Distribution of afterslip along the imperial fault. In *The Imperial Valley Earthquake of October 15, 1979, US Geol. Surv. Prof. Pap.* 1254:193–203
Hartzell SH, Heaton TH. 1983. Inversion of strong ground motion and teleseismic waveform data for the fault rupture history of the 1979 Imperial Valley, California earthquake. *Bull. Seismol. Soc. Am.* 73:53–83
Heaton TH. 1990. Evidence for and implications of self-healing pulses of slip in earthquake rupture. *Phys. Earth Planet Inter.* 64:1–20
Heimpel M. 1996. Earthquake size-frequency relations from an analytical stochastic rupture model. *J. Geophys. Res.* 101:22435–48
Heimpel M. 1997. Critical behaviour and the evolution of fault strength during earthquake cycles. *Nature* 388:856–58
Heki K, Miyazaki S, Tsuji H. 1997. Silent fault slip following an interplate thrust earthquake at the Japan trench. *Nature* 386:595–98
Hickman S, Sibson R, Bruhn R. 1995. Introduction to special section: mechanical involvement of fluids in faulting. *J. Geophys. Res.* 100:12831–40
Hickman SH. 1991. Stress in the lithosphere and the strength of active faults. *Rev. Geophys. Suppl.* pp. 759–75
Horowitz FG. 1988. Mixed state variable friction laws; some implications for experiments and stability analysis. *Geophys. Res. Lett.* 15:1243–46
Horowitz FG, Ruina A. 1989. Slip patterns in a spatially homogeneous fault model. *J. Geophys. Res.* 93:10279–98
Huang J, Turcotte DL. 1992. Chaotic seismic faulting with a mass-spring model and velocity weakening friction. *Pure Appl. Geophys.* 138:509–89
Ihmlé PF. 1996. Monte Carlo slip inversion in the frequency domain: application to the 1992 Nicaragua slow earthquake. *Geophys. Res. Lett.* 23:913–16
Ihmlé PF, Harabaglia P, Jordan TH. 1993. Teleseismic detection of a slow presursor to the great 1989 Macquarie Ridge earthquake. *Science* 261:177
Ihmlé PF, Jordan TH. 1994. Teleseismic search for slow precursors to large earthquakes. *Science* 266:1547–51
Iio Y. 1992. Slow initial phase of the P-wave velocity pulse generated by microearthquakes. *Geophys. Res. Lett.* 19:477–80
Jackson DD, et al. 1995. Seismic hazards in southern California: probable earthquakes 1994 to 2024. *Bull. Seismol. Soc. Am.* 85:379–439
Johnson T. 1981. Time-dependent friction of granite: implications for precursory slip on faults. *J. Geophys. Res.* 86:6017–28

Kanamori H. 1994. Mechanics of earthquakes. *Annu. Rev. Earth Planet. Sci.* 22:207–37
Kanamori H, Allen CR. 1986. Earthquake repeat time and average stress drop. See Das et al 1986, 37:227–36
Kanamori H, Kikuchi M. 1993. The 1992 Nicaragua earthquake: a slow tsunami earthquake associated with subducted sediments. *Nature* 361:714–16
Karner SL, Marone C, Evans B. 1997. Laboratory study of fault healing and lithification in simulated fault gouge under hydrothermal conditions. *Tectonophysics* 277:41–55
Kato N, Hirasawa T. 1996. Effects of strain rate and strength nonuniformity on the slip nucleation process; a numerical experiment. *Tectonophysics* 256:299–311
Kato N, Yamamoto K, Hirasawa T. 1994. Microfracture processes in the breakdown zone during dynamic shear rupture inferred from laboratory observation of near-fault high-frequency strong motion. *Pure Appl. Geophys.* 142:713–34
Kato N, Yamamoto K, Yamamoto H, Hirasawa T. 1992. Strain-rate effects on frictional strength and the slip nucleation process. *Tectonophysics* 211:269–82
Kato N, Yamamoto K, Yamamoto H, Hirasawa T. 1993. A stress-corrosion model for strain-rate dependence of the frictional strength of rocks. *Int. J. Rock Mech. Mining Sci.* 30:551–54
Kawasaki I, Asai Y, Tamura Y, Sagiya T, Mikami N, et al. 1995. The 1992 Sanriku-Oki, Japan, ultra-slow earthquake. *J. Phys. Earth* 43:105–16
Kilgore BD, Blanpied ML, Dieterich JH. 1993. Velocity-dependent friction of granite over a wide range of conditions. *Geophys. Res. Lett.* 20:903–6
Lienkaemper JJ, Borchardt G, Lisowski M. 1991. Historic creep rate and potential for seismic slip along the Hayward fault, California. *J. Geophys. Res.* 96:1826–83
Linde AT, Gladwin MT, Johnston MJS, Gwyther RL, Bilham RG. 1996. A slow earthquake sequence on the San Andreas fault. *Nature* 383:65–68
Linker MF, Dieterich JH. 1992. Effects of variable normal stress on rock friction: observations and constitutive equations. *J. Geophys. Res.* 97:4923–40
Lockner DA, Summers R, Byerlee JD. 1986. Effects of temperature and sliding rate on frictional strength of granite. *Pure Appl. Geophys.* 124:445–69
Logan JM. 1978. Creep, stable sliding, and premonitory slip. *Pure Appl. Geophys.* 116:773–89
Logan JM, Dengo CA, Higgs NG, Wang ZZ. 1992. Fabrics of experimental fault zones: their development and relationship to mechanical behavior. In *Fault Mechanics and Transport Properties of Rocks*, ed. B Evans, Tf Wong, pp. 33–67. London: Academic
Logan JM, Friedman M, Higgs N, Dengo C, Shimamoto T. 1979. Experimental studies of simulated gouge and their application to studies of natural fault zones. In *Analyses of Actual Fault Zones in Bedrock. US Geol. Surv. Open File Rep.* 1239:305–43
Lorenzetti E, Tullis TE. 1989. Geodetic predictions of a strike-slip fault model: implications for intermediate-and short-term earthquake prediction. *J. Geophys. Res.* 94:12343–61
Lorig LJ, Hobbs BE. 1990. Numerical modelling of slip instability using the distinct element method with state variable friction laws. *Int. J. Rock Mech. Mining Sci.* 27:525–34
Ma S, Toshihiko S. 1995. Effect of dehydration of montmorillonite on constitutive behavior of friction. *Seismol. Geol.* 17:297–304
Main I. 1996. Statistical physics, seismogenesis, and seismic hazards. *Rev. Geophys.* 34:433–62
Marone C. 1991. A note on the stress-dilatancy relation for simulated fault gouge. *Pure Appl. Geophys.* 137:409–19
Marone C. 1993. Micromechanics of rate- and state-dependent friction in simulated fault gouge. *Eos, Trans. Am. Geophys. Union* 74:296
Marone C. 1995. Fault zone strength and failure criteria. *Geophys. Res. Lett.* 22:723–26
Marone C. 1998. The effect of loading rate on static friction and the rate of fault healing during the earthquake cycle. *Nature* 391:69–72
Marone C, Cox SJD. 1994. Scaling of rock friction constitutive parameters: the effects of surface roughness and cumulative offset on friction of gabbro. *Pure Appl. Geophys.* 143:359–86
Marone C, Hobbs BE, Ord A. 1992. Coulomb constitutive laws for friction: constrasts in frictional behavior for distributed and localized shear. *Pure Appl. Geophys.* 139:195–214
Marone C, Kilgore B. 1993. Scaling of the critical slip distance for seismic faulting with shear strain in fault zones. *Nature* 362:618–21
Marone C, Raleigh CB, Scholz CH. 1990. Frictional behavior and constitutive modeling of simulated fault gouge. *J. Geophys. Res.* 95:7007–25
Marone C, Scholz CH. 1988. The depth of seismic faulting and the upper transition from stable to unstable slip regimes. *Geophys. Res. Lett.* 15:621–24
Marone C, Scholz CH. 1989. Particle-size distribution and microstructures within simulated fault gouge. *J. Struct. Geol.* 11:799–14
Marone C, Scholz CH, Bilham R. 1991. On the

mechanics of earthquake afterslip. *J. Geophys. Res.* 96:8441–52
Marone C, Vidale JE, Ellsworth W. 1995. Fault healing inferred from time dependent variations in source properties of repeating earthquakes. *Geophys. Res. Lett.* 22:3095–98
Mase CW, Smith L. 1987. Effects of frictional heating on the thermal, hydrologic, and mechanical response of a fault. *J. Geophys. Res.* 92:6249–72
Mavko GM. 1981. Mechanics of motion on major faults. *Annu. Rev. Earth Planet. Sci.* 9:81–111
McGuire JJ, Ihmle PF, Jordan TH. 1996. Time-domain observations of a slow precursor to the 1994 Romance transform earthquake. *Science* 274:82–85
Melosh HJ. 1979. Acoustic fluidization: a new geological process? *J. Geophys. Res.* 84:7513–20
Melosh HJ. 1996. Dynamical weakening of faults by acoustic fluidization. *Nature* 379: 601–6
Miller SA. 1996. Fluid-mediated influence of adjacent thrusting on the seismic cycle at Parkfield. *Nature* 381:799–802
Miller SA, Nur A, Olgaard DL. 1996. Earthquakes as a coupled shear stress - high pore pressure dynamical system. *Geophys. Res. Lett.* 23:197–200
Moore DE, Lockner DA, Summers R, Ma S, Byerlee JD. 1996. Strength of chrysotile-serpentinite gouge under hydrothermal conditions; can it explain a weak San Andreas fault? *Geology* 24:1041–44
Mora P, Place P. 1994. Simulation of the frictional stick-slip instability. *Pure Appl. Geophys.* 143:61–87
Morrow CA, Byerlee JD. 1989. Experimental studies of compaction and dilatancy during frictional sliding on faults containing gouge. *J. Struct. Geol.* 11:815–25
Morrow CA, Lockner D, Byerlee JD. 1986. Velocity- and time-dependent stress transients in simulated fault gouge. In *Engineering in Complex Rock Formations*, pp. 142–48. Beijing: Int. Soc. Rock. Mech.
Myers CH, Shaw BE, Langer JS. 1996. Slip complexity in a two dimensional crustal plane model. *Phys. Rev. Lett.* 77:972
Nakatani M, Mochizuki H. 1996. Effects of shear stress applied to surface in stationary contact on rock friction. *Geophys. Res. Lett.* 23:869–72
Nason R, Weertman J. 1973. A dislocation theory analysis of fault creep events. *J. Geophys. Res.* 78:7745–51
Ohnaka M. 1973. Experimental studies of stick-slip and their application to the earthquake source mechanism. *J. Phys. Earth* 21:285–303
Ohnaka M. 1986. Dynamic breakdown processes and the generating mechanism for high frequency elastic radiation during stick-slip instabilities. See Das et al 1986, 37:13–24
Ohnaka M. 1996. Nonuniformity of the constitutive law parameters for shear rupture and quasistatic nucleation to dynamic rupture: a physical model of earthquake generation processes. *Proc. Natl. Acad. Sci.* 93:3795–802
Ohnaka M, Kuwahara Y. 1990. Characteristic features of local breakdown near a crack-tip in the transition zone from nucleation to dynamic rupture during stick-slip shear failure. *Tectonophysics* 175:197–220
Ohnaka M, Yamashita T. 1989. A cohesive zone model for dynamic shear faulting based on experimentally inferred constitutive relation and strong motion source parameters. *J. Geophys. Res.* 94:4089–104
Okubo PG. 1989. Dynamic rupture modeling with laboratory-derived constitutive relations. *J. Geophys. Res.* 94:12321–35
Okubo PG, Dieterich JH. 1984. Effects of physical fault properties on frictional instabilities produced on simulated faults. *J. Geophys. Res.* 89:5817–27
Olsson WA. 1988. The effects of normal stress history on rock friction. In *Key Questions in Rock Mechanics*, ed. PA Cundall, RL Sterling, AM Starfield, pp. 111–17. Rotterdam: Balkema
Perrin G, Rice JR, Zheng G. 1995. Self-healing slip pulse on a frictional surface. *J. Mech. Phys. Solids* 43:1461–95
Pollitz FF. 1997. Gravitational viscoelastic post-seismic relaxation on a layered spherical Earth. *J. Geophys. Res.* 102:17921–41
Power WL, Tullis TE. 1992. The contact between opposing fault suraces at Dixie Valley, Nevada, and implications for fault mechanics. *J. Geophys. Res.* 97:15425–36
Power WL, Tullis TE, Weeks JD. 1988. Roughness and wear during brittle faulting. *J. Geophys. Res.* 93:15268–78
Quin H. 1990. Dynamic stress drop and rupture dynamics of the October 15, 1979, Imperial Valley, California, earthquake. *Tectonophysics* 175:93–117
Rabinowicz E. 1951. The nature of static and kinetic coefficients of friction. *J. Appl. Phys.* 22:1373–79
Rabinowicz E. 1958. The intrinsic variables affecting the stick-slip process. *Proc. Phys. Soc. London* 71:668–75
Raleigh CB, Healy JH, Bredehoeft JD. 1976. An experiment in earthquake control at Rangely, CO. *Science* 191:1230–37
Raleigh CB, Marone C. 1986. Dilatancy of quartz gouge in pure shear. In *Mineral and Rock Deformation: Laboratory Studies*, ed. BE Hobbs, HC Heard, Am. Geophys. Union

Monogr., 36:1–10. Washington, DC: Am. Geophys. Union
Reinen LA, Tullis TE, Weeks JD. 1992. Two-mechanism model for frictional sliding of serpentine. *Geophys. Res. Lett.* 19:535–38
Reinen LA, Weeks JD. 1993. Determination of rock friction constitutive parameters using an iterative least-squares inversion method. *J. Geophys. Res.* 98:15937–50
Reinen LA, Weeks JD, Tullis TE. 1991. The frictional behavior of serpentinite: implications for aseismic creep on shallow crustal faults. *Geophys. Res. Lett.* 18:1921–24
Reinen LA, Weeks JD, Tullis TE. 1994. The frictional behavior of lizardite and antigorite serpentinites: experiments, constitutive models and implications for natural faults. *Pure Appl. Geophys.* 143:317–58
Rice JR. 1983. Constitutive relations for fault slip and earthquake instabilities. *Pure Appl. Geophys.* 121:443–75
Rice JR. 1992. Fault stress states, pore pressure distributions, and the weakness of the San Andreas Fault. In *Fault Mechanics and Transport Properties of Rocks*, ed. B Evans, Tf Wong, pp. 475–504. London: Academic
Rice JR. 1993. Spatio-temporal complexity of slip on a fault. *J. Geophys. Res.* 98:9885–907
Rice JR, Ben-Zion Y. 1996. Slip complexity in earthquake fault models. *Proc. Natl. Acad. Sci. USA* 93:3811
Rice JR, Gu JC. 1983. Earthquake aftereffects and triggered seismic phenomena. *Pure Appl. Geophys.* 121:187–219
Rice JR, Ruina AL. 1983. Stability of steady frictional slipping. *J. Appl. Mech.* 105:343–49
Roy M, Marone C. 1996. Earthquake nucleation on model faults with rate and state dependent friction: the effects of inertia. *J. Geophys. Res.* 101:13919–32
Rudnicki JW. 1980. Fracture mechanics applied to the Earth's crust. *Annu. Rev. Earth Planet. Sci.* 8:489–525
Rudnicki JW. 1988. Physical models of earthquake instability and precursory processes. *Pure Appl. Geophys.* 126:531–54
Ruina A. 1983. Slip instability and state variable friction laws. *J. Geophys. Res.* 88:10359–70
Rundle J, Jackson DD. 1977. A viscoelastic relaxation model for postseismic deformation from the San Francisco Earthquake of 1906. *Pure Appl. Geophys.* 115:401–11
Rundle JB, Klein W, Gross S. 1996. Dynamics of a traveling density wave model for earthquakes. *Phys. Rev. Lett.* 76:4285–89
Rutter EH, Maddock RH, Hall SH, White SH. 1986. Comparative microstructures of natural and experimentally produced clay bearing fault gouges. *Pure Appl. Geophys.* 124:3–29
Sammis CG, Biegel R. 1989. Fractals, fault gouge and friction. *Pure Appl. Geophys.* 131:255–71
Sammis CG, King G, Biegel R. 1987. The kinematics of gouge deformation. *Pure Appl. Geophys.* 125:777–812
Sammis CG, Steacy SJ. 1994. The micromechanics of friction in a granular layer. *Pure Appl. Geophys.* 143:777–94
Schmittbuhl J, Vilotte JP, Roux S. 1996. Velocity weakening friction: a renormalization approach. *J. Geophys. Res.* 101:13911–17
Scholz CH. 1987. Wear and gouge formation in brittle faulting. *Geology* 15:493–95
Scholz CH. 1988a. The critical slip distance for seismic faulting. *Nature* 336:761–63
Scholz CH. 1988b. The brittle-plastic transition and the depth of seismic faulting. In *Detachment and Shear*, ed. H Zankl, J Delliere, A Prashnowsky, Geol. Rundsch., 77:319–28
Scholz CH. 1989. Mechanics of faulting. *Annu. Rev. Earth Planet. Sci.* 17:309–34
Scholz CH. 1990. *The Mechanics of Earthquakes and Faulting.* New York: Cambridge Univ. Press. 439 pp.
Scholz CH, Aviles CA, Wesnousky SG. 1986. Scaling differences between large interplate and intraplate earthquakes. *Bull. Seismol. Soc. Am.* 76:65–70
Scholz CH, Campos J. 1995. On the mechanism of seismic decoupling and back arc spreading at subduction zones. *J. Geophys. Res.* 100:22103–15
Scholz CH, Engelder JT. 1976. The role of asperity indentation and ploughing in rock friction: I. Asperity creep and stick slip. *Int. J. Rock Mech. Mining Sci.* 13:149–54
Scholz CH, Molnar P, Johnson T. 1972. Detailed studies of frictional sliding of granite and implications for the earthquake mechanism. *J. Geophys. Res.* 77:6392–406
Scholz CH, Wyss M, Smith SW. 1969. Seismic and aseismic slip on the San Andreas fault. *J. Geophys. Res.* 74:2049–69
Schulz SS. 1984. Response of USGS creepmeters near Hollister to the April 24, 1984, Morgan Hill Earthquake. *Open File Rep. US Geol. Surv.* pp. 64–71
Schulz SS, Mavko GM, Burford RO, Stuart WD. 1982. Long-term fault creep observations in central California. *J. Geophys. Res.* 87:6977–82
Scott DR. 1996. Seismicity and stress rotation in a granular model of the brittle crust. *Nature* 381:592–95
Scott DR, Marone C, Sammis CG. 1994. The apparent friction of granular fault gouge in sheared layers. *J. Geophys. Res.* 99:7231–46
Segall P, Du YJ. 1993. How similar were the 1934 and 1966 Parkfield earthquakes? *J. Geophys. Res.* 98:4527–38
Segall P, Rice JR. 1995. Dilatancy, compaction,

and slip instability of a fluid infiltrated fault. *J. Geophys. Res.* 100:22155–73
Sharp RV, et al. 1982. Surface faulting in the central Imperial Valley. In *The Imperial Valley Earthquake of October 15, 1979, US Geol. Surv. Prof. Pap.* 1254:119–44
Sharp RV, Budding KE, Boatwright J, Ader MJ, Bonilla MG, et al. 1989. Surface faulting along the Superstition Hills fault zone and nearby faults associated with the earthquakes of 24 November 1987. *Bull. Seismol. Soc. Am.* 79:252–81
Shaw BE. 1994. Complexity in a spatially uniform continuum fault model. *Geophys. Res. Lett.* 21:1983–86
Shaw BE. 1995. Frictional weakening and slip complexity in earthquake faults. *J. Geophys. Res.* 100:18239–51
Shaw BE, Carlson JM, Langer JS. 1992. Patterns of seismic activity preceding large earthquakes. *J. Geophys. Res.* 97:479–88
Shen ZK, Jackson DD, Feng Y, Cline M, Kim M, et al. 1994. Postseismic deformation following the Landers Earthquake, California, 28 June 1992. *Bull. Seismol. Soc. Am.* 84:780–91
Shibazaki B, Matsu'ura M. 1992. Spontaneous processes for nucleation, dynamic propagation, and stop of earthquake rupture. *Geophys. Res. Lett.* 19:189–92
Shibazaki B, Matsu'ura M. 1995. Foreshocks and pre-events associated with the nucleation of large earthquakes. *Geophys. Res. Lett.* 22:1305–8
Shimamoto T, Logan JM. 1981. Effects of simulated fault gouge on the sliding behavior of Tennessee sandstone: nonclay gouges. *J. Geophys. Res.* 86:2902–14
Shimamoto T, Logan JM. 1986. Velocity-dependent behavior of simulated halite shear zones: an analog for silicates. See Das et al 1986, 37:49–63
Sibson RH. 1986. Earthquakes and rock deformation in crustal fault zones. *Annu. Rev. Earth Planet. Sci.* 14:149–75
Sleep NH. 1994. Grain size and chemical controls on the ductile properties of mostly frictional faults at low-temperature hydrothermal conditions. *Pure Appl. Geophys.* 143:41–60
Sleep NH. 1995a. Ductile creep, compaction, and rate and state dependent friction within major fault zones. *J. Geophys. Res.* 100:13065–80
Sleep NH. 1995b. Frictional heating and the stability of rate and state dependent frictional sliding. *Geophys. Res. Lett.* 22:2785–88
Sleep NH. 1997. Application of a unified rate and state friction theory to the mechanics of fault zones with strain localization. *J. Geophys. Res.* 102:2875–95
Sleep NH, Blanpied ML. 1992. Creep, compaction and the weak rheology of major faults. *Nature* 359:687–92
Sleep NH, Blanpied ML. 1994. Ductile creep and compaction: a mechanism for transiently increasing fluid pressure in mostly sealed fault zones. *Pure Appl. Geophys.* 143:9–40
Smith SW, Wyss M. 1968. Displacement on the San Andreas fault subsequent to the 1966 Parkfield earthquake. *Bull. Seismol. Soc. Am.* 58:1955–73
Solberg P, Byerlee J. 1984. A note on the rate sensitivity of frictional sliding of Westerly granite. *J. Geophys. Res.* 89:4203–5
Sornette D, Knopoff L, Kagan YY, Vanneste C. 1996. Rank-ordering statistics of extreme events: application to the distribution of large earthquakes. *J. Geophys. Res.* 101:13833–93
Spray JG. 1993. Viscosity determinations of some frictionally generated silicate melts: implications for fault zone rheology at high strain rates. *J. Geophys. Res.* 98:8053–68
Steacy S, Sammis CG. 1992. A damage mechanics model for fault zone friction. *J. Geophys. Res.* 97:587–94
Stesky R. 1978. Mechanisms of high temperature frictional sliding in Westerly granite. Can. *J. Earth Sci.* 15:361–75
Stesky RM, Hannan SS. 1989. A new theory for the static contact between rough, unmated surfaces in non-elastically deforming rock and its implication for rock friction. *J. Struct. Geol.* 11:787–98
Stuart WD, Tullis TE. 1995. Fault model for preseismic deformation at Parkfield, California. *J. Geophys. Res.* 100:24079–99
Sylvester AG. 1993. Investigation of nearfield postseismic slip following the M_w 7.3 Landers earthquake sequence of 28 June 1992, California. *Geophys. Res. Lett.* 20:1079–82
Takashi M. 1992. Numerical simulation of three-dimensional faulting process with heterogeneous rate- and state-dependent friction. *Tectonophysics* 211:223–32
Teufel LW. 1981. Pore volume changes during frictional sliding of simulated faults. In *Mechanical Behavior of Crustal Rocks*, ed. NL Carter, M Friedman, JM Logan, DW Sterns, Am. Geophys. Union Monogr., 24:135–45. Washington, DC: Am. Geophys. Union
Teufel LW, Logan JM. 1978. Effect of displacement rate on the real area of contact and temperature generated during frictional sliding of Tennessee sandstone. *Pure Appl. Geophys.* 116:840–72
Tse ST, Rice JR. 1986. Crustal earthquake instability in relation to the depth variation of frictional slip properties. *J. Geophys. Res.* 91:9452–72
Tsutsumi A, Shimamoto T. 1997. High-velocity frictional characteristics of gabbro. *Geophys. Res. Lett.* 24:699–702

Tullis TE. 1988. Rock friction constitutive behavior from laboratory experiments and its implications for an earthquake prediction field monitoring program. *Pure Appl. Geophys.* 126:555–88

Tullis TE. 1996. Rock friction and its implications for earthquake prediction examined via models of Parkfield earthquakes. *Proc. Natl. Acad. Sci. USA* 93:3803–10

Tullis TE, Beeler NM, Weeks JD. 1993. The nature of the evolution effect in rock friction. *Eos, Trans. Am. Geophys. Union* 74:296

Tullis TE, Weeks JD. 1986. Constitutive behavior and stability of frictional sliding of granite. *Pure Appl. Geophys.* 124:383–414

Vidale JE, Ellsworth W, Cole A, Marone C. 1994. Rupture variation with recurrence interval in eighteen cycles of a small earthquake. *Nature* 368:624–26

Wald DJ, Heaton TH. 1994. Spatial and temporal distribution of slip for the 1992 Landers, California, earthquake. *Bull. Seismol. Soc. Am.* 84:668–91

Wald DJ, Helmberger DV, Hartzell SH. 1990. Rupture process of the 1987 Superstition Hills earthquake from the inversion of strong-motion data. *Bull. Seismol. Soc. Am.* 80:1079–98

Wang W, Scholz CH. 1994. Micromechanics of the velocity and normal stress dependence of rock friction. *Pure Appl. Geophys.* 143:303–16

Wang W, Scholz CH. 1995. Micromechanics of rock friction, 3. Quantitative modeling of base friction. *J. Geophys. Res.* 100:4243–48

Weeks JD. 1993. Constitutive laws for high-velocity frictional sliding and their influence on stress drop during unstable slip. *J. Geophys. Res.* 98:17637–48

Weeks JD, Byerlee JD. 1978. Preliminary investigation of volume changes in crushed granite preceding stick-slip failure. *Geophys. Res. Lett.* 5:832–34

Weeks JD, Tullis TE. 1985. Frictional sliding of dolomite: a variation in constitutive behavior. *J. Geophys. Res.* 90:7821–26

Wennerberg L, Sharp RV. 1997. Bulk-friction modeling of afterslip and the modified Omori law. *Tectonophysics* 277:109–36

Wesnousky SG. 1988. Seismological and structural evolution of strike-slip faults. *Nature* 335:340–43

Wesnousky SG. 1990. Seismicity as a function of cumulative geologic offset: some observations from southern California. *Bull. Seismol. Soc. Am.* 80:1374–81

Wesnousky SG. 1994. The Gutenberg-Richter or characteristic earthquake distribution, which is it? *Bull. Seismol. Soc. Am.* 84:1940–59

Wesson RL. 1988. Dynamics of fault creep. *J. Geophys. Res.* 93:8929–51

Williams PL, Magistrale HW. 1989. Slip along the Superstition Hills fault associated with the 24 November 1987 Superstition Hills, California, earthquake. *Bull. Seismol. Soc. Am.* 79:390–410

Wong Tf, Gu Y, Yanagidani T, Zhao Y. 1992. Stabilization of faulting by cumulative slip. In *Fault Mechanics and Transport Properties of Rock*, ed. B Evans, Tf Wong, pp. 119–43. London: Academic

Wong Tf, Zhao Y. 1990. Effects of load point velocity on frictional instability behavior. *Tectonophysics* 175:177–95

Yamashita T, Ohnaka M. 1991. Nucleation process of unstable rupture in the brittle regime: a theoretical approach based on experimentally inferred relations. *J. Geophys. Res.* 96:8351–67

Yoshioka N, Scholz CH. 1989a. Elastic properties of contacting surfaces under normal and shear loads, 1. Theory. *J. Geophys. Res.* 94:17681–90

Yoshioka N, Scholz CH. 1989b. Elastic properties of contacting surfaces under normal and shear loads, 2. Comparison of theory with experiment. *J. Geophys. Res.* 94:17691–700